

ISTANBUL TECHNICAL UNIVERSITY ★ GRADUATE SCHOOL OF SCIENCE
ENGINEERING AND TECHNOLOGY

**GEOID MODELING BY THE LEAST SQUARES
MODIFIED HOTINE FORMULA USING VORONOI CELL STRUCTURES**



M.Sc. THESIS

Fatima Feyza SAKIL

Department of Geomatics Engineering

Geomatics Engineering Programme

JUNE 2018

**GEOID MODELING BY THE LEAST SQUARES
MODIFIED HOTINE FORMULA USING VORONOI CELL STRUCTURES**

M.Sc. THESIS

**Fatıma Feyza SAKIL
(501161614)**

Department of Geomatics Engineering

Geomatics Engineering Programme

Thesis Advisor: Assoc. Prof. Dr. Serdar EROL

JUNE 2018

İSTANBUL TEKNİK ÜNİVERSİTESİ ★ FEN BİLİMLERİ ENSTİTÜSÜ

**VORONOI HÜCRE YAPILARI ARACILIĞIYLA HOTİNE İNTEGRALİNİN
EN KÜÇÜK KARELER MODİFİKASYONU İLE GEOİT BELİRLEME**

YÜKSEK LİSANS TEZİ

**Fatma Feyza SAKİL
(501161614)**

Geomatik Mühendisliği Anabilim Dalı

Geomatik Mühendisliği Programı

Tez Danışmanı: Assoc. Prof. Dr. Serdar EROL

HAZİRAN 2018

Fatma Feyza SAKIL, a M.Sc. student of ITU Graduate School of Science Engineering and Technology 501161614 successfully defended the thesis entitled “GEOID MODELING BY THE LEAST SQUARES MODIFIED HOTINE FORMULA USING VORONOI CELL STRUCTURES ”, which she prepared after fulfilling the requirements specified in the associated legislations, before the jury whose signatures are below.

Thesis Advisor : **Assoc. Prof. Dr. Serdar EROL**
Istanbul Technical University

Jury Members : **Prof. Dr. Ergin TARI**
Istanbul Technical University

Assoc. Prof. Dr. Ramazan Alpay ABBAK
Selcuk University

.....

Date of Submission : **4 May 2018**
Date of Defense : **11 June 2018**



FOREWORD

First and foremost, I would like to thank my supervisor Dr. Serdar Erol for his support and patience. He provided a suitable working environment, the powerful hardware needed for computations and most importantly shared his experience and time for my learning progress. He cheered me on focusing on each detail and encouraged me to take my initial steps through the academic world.

Secondly, I am highly grateful to my unofficial supervisors Dr. Artu Ellmann and Dr. Bihter Erol. Dr. Ellmann accepted me as an exchange student at Tallinn University of Technology, Estonia; provided all necessary information and documents during the acceptance process. He guided me to clarify the topic of my thesis, introduced me to the Least Squares Modification of Hotine Integral for regional geoid determination and encouraged me to test empirical methods. He also provided a software to calculate the least squares modification parameters of for both Stokes and Hotine procedures.

Dr. Bihter Erol shared her experience on gravimetric geoid modeling, discussed the results of each step of the study and revised all the content and papers submitted to the related academic events. Not to mention her remote support and care while I was in Estonia, dealing with dark weather and trying to motivate myself.

Thirdly, I am grateful to Dr. Ramazan Alpay Abbak for sharing his LSMSSOFT software package which was beneficial while I was trying to find the problematic parts on my algorithm and applied readjustments.

I also would like to thank my dearest friends and colleagues Mustafa Serkan Işık and Öykü Koç who were extremely supportive both in scientific and psychological manners during the study I conducted which required to be committed for a long period of time. They made a significant contribution while solving the problems I encountered and stayed with me during the late nights in the office. We, as "The Gravity Research Group" in Istanbul Technical University (ITU-GRG) had long discussions and brought out brand new questions need to be revealed in future studies. Aside from their support Serkan also introduced me GMT and LaTeX software packages which are rather advantageous and efficient tools for data manipulation and script editing.

Additively, I am obliged to my caring friend and colleague Payam Shokrzadeh who came as a rescue while I was trying to evaluate the discrete data for days and helped me modify my algorithm to be suitable for parallel processing.

I am also grateful for my close friend, former teammate Neziha Yılmaz for her continuous support and helpfulness. I will remember the times I spent in her place and the good (sometimes dark) sense of humor of her that cheered me on each day.

Last but not least, I owe many thanks to my family and to the rest of my friends for their patience and support. They tried to comfort me and ease my tension during the whole period. They even listened to my unending grumbles and kindly motivated me towards the final stage.

11 June 2018

Fatıma Feyza SAKIL
(Geomatics Engineer)



TABLE OF CONTENTS

	<u>Page</u>
FOREWORD	viii
TABLE OF CONTENTS	ix
ABBREVIATIONS	xi
SYMBOLS	xiii
LIST OF TABLES	xv
LIST OF FIGURES	xvii
SUMMARY	xix
ÖZET	xxi
1. INTRODUCTION	1
1.1 Background.....	1
1.2 Purpose of the Study	3
1.3 Outline.....	3
2. METHODOLOGY	5
2.1 Gravity Potential and Geoid	5
2.2 Normal Gravity.....	6
2.3 Gravity Anomaly	7
2.4 Gravity Disturbance	8
2.5 Geoid Modeling with KTH Method	9
2.6 Least Squares Modification of Hotine’s Function.....	11
2.6.1 Additive corrections.....	13
2.6.1.1 Combined topographic correction	13
2.6.1.2 Combined downward continuation correction.....	14
2.6.1.3 Combined atmospheric correction	15
2.6.1.4 Combined ellipsoidal correction.....	15
2.7 Singularity Problem.....	16
2.7.1 The elimination of singularity for grid-wise evaluation.....	17
2.7.2 The elimination of singularity for point-wise evaluation.....	18
3. DATA PREPARATION	23
3.1 Terrestrial Gravity Dataset	24
3.1.1 Input gravity quantities	25
3.1.2 Voronoi diagrams	29
3.2 GNSS/Leveling Benchmarks.....	32
3.3 Digital Elevation Model.....	33
3.4 Global Geopotential Model.....	34
4. NUMERICAL RESULTS	35
4.1 Determination of Modification Parameters	35
4.2 LSMHA Geoid with Components.....	36

4.3 Validation and Comparison of Resulting Geoid Models..... 41

5. COMPUTATIONAL DIFFICULTIES..... 45

6. CONCLUSIONS 49

REFERENCES..... 53

CURRICULUM VITAE..... 57



ABBREVIATIONS

BLS	: Biased Least Squares
CBA	: Complete Bouguer Anomaly
ETRS89	: European Terrestrial Reference Frame 1989
DEM	: Digital Elevation Model
GGM	: Global Geopotential Model
GMT	: The Generic Mapping Tools
GNSS	: Global Navigational Satellite System
GOCE	: Gravity field and steady state Ocean Circulation Explorer
GOCO	: Gravity Observation Combination
GBVP	: Geodetic Boundary Value Problem
GRACE	: Gravity Recovery and Climate Experiment
LSC	: Least Squares Collocation
GRS80	: Geodetic Reference System 1980
IGN	: Institut Géographique National
KTH	: Kungliga Tekniska Högskolan (Royal Institute of Technology)
LSMH	: Least Squares Modification of Hotine's Formula
LSMHA	: Least Squares Modification of Hotine's Formula with Additive Corrections
LSMS	: Least Squares Modification of Stokes' Formula
LSMSA	: Least Squares Modification of Stokes' Formula with Additive Corrections
OLS	: Optimum Least Squares
RCR	: Remove Compute Restore
RMS	: Root Mean Square
STD	: Standard Deviation
ULS	: Unbiased Least Squares



SYMBOLS

a	: semi-major axis of the reference ellipsoid
b	: semi-minor axis of the reference ellipsoid
e^2	: eccentricity of the reference ellipsoid
R	: mean Earth radius
φ	: latitude
ϕ	: geocentric latitude
λ	: longitude
r	: geocentric radius
H	: orthometric height
H^N	: normal height
h	: ellipsoidal height
N	: geoid height
\hat{N}	: geoid estimator
\tilde{N}	: approximate geoid
ζ	: quasigeoid height / height anomaly
ζ^0	: approximate value of height anomaly
γ_{Q_0}	: normal gravity of the reference ellipsoid
γ_Q	: normal gravity reduced to telluroid
γ_a	: normal gravity on equator
γ_b	: normal gravity on poles
Δg_0	: classical gravity anomaly
Δg	: surface gravity anomaly
Δg^{SBA}	: simple Bouger gravity anomaly
Δg^{CBA}	: complete Bouger gravity anomaly
δg^{TC}	: terrain correction
δg	: gravity disturbance
δg_n	: spherical harmonic representation of gravity anomaly
Δg_n	: spherical harmonic representation of gravity disturbance
ψ	: spherical distance between the computation point and the integration points
ψ_0	: radius of the integration cap
M	: upper limit of global geopotential model
L	: upper limit of Stokes/Hotine function
$H(\psi)$: Hotine function
$H^L(\psi)$: Modified Hotine function
$S(\psi)$: Stokes function
$S^L(\psi)$: Modified Stokes function
σ	: unit sphere
σ_0	: integration cap

c_n^2	: gravity signal degree variances
dc_n^2	: GGM error degree variances
Q_n	: un-modified truncation coefficients
Q_n^L	: modified truncation coefficients
s_n	: modification parameters
b_n	: modification parameters
m	: spherical harmonic degree
n	: spherical harmonic order
G	: Newton's gravitational constant
$\overline{C}_{nm}, \overline{C}_{nm}^W$: fully normalized spherical harmonic coefficient
\overline{S}_{nm}	: fully normalized spherical harmonic coefficient
\overline{U}_{nm}^U	: fully normalized even zonal harmonics of normal potential
$P_n \cos(\psi)$: un-normalized Legendre polynomials of spherical harmonic degree n
$\overline{P}_{nm}(\sin \phi)$: fully normalized Legendre polynomials of spherical harmonic degree n, order m
R_{nk}	: function of the integration radius ψ_0
\overline{HC}_{nm}	: spherical harmonic model coefficients for Earth's elevation
\overline{HS}_{nm}	: spherical harmonic model coefficients for Earth's elevation
H_n	: Laplace surface harmonics of the topographic height
ρ	: topographic density
ρ_A	: atmospheric density
δN_{ATM}	: combined atmospheric correction
δN_{COMB}	: combined topographic correction
δN_{DWC}	: combined downward continuation correction
δN_{ELL}	: combined ellipsoidal correction
δg_{en}	: Laplace harmonics of the ellipsoidal correction

LIST OF TABLES

	<u>Page</u>
Table 2.1 : Comparison of LSMSA (Stokes) and LSMHA (Hotine) methods	19
Table 2.2 : Comparison of additive corrections for LSMSA (Stokes) and LSMHA (Hotine) methods	20
Table 2.3 : Comparison of additive corrections for LSMSA (Stokes) and LSMHA (Hotine) methods (continued)	21
Table 3.1 : List of tested GGMs	34
Table 4.1 : Statistical results of geoid models calculated by different parameters	36
Table 4.2 : Selected parameters	36
Table 4.3 : Statistical results of the final geoid models: before fit (unit: m)	42
Table 4.4 : Statistical results of the final geoid models: after fit (unit: m)...	42



LIST OF FIGURES

	<u>Page</u>
Figure 1.1 : Height reference surfaces.....	1
Figure 2.1 : Illustration of the relevant surfaces.....	7
Figure 2.2 : Unmodified Hotine function for the spherical distances calculated in the truncation cap	16
Figure 3.1 : Auvergne area	23
Figure 3.2 : Auvergne terrestrial gravity network	24
Figure 3.3 : Auvergne gravity disturbances.....	25
Figure 3.4 : Auvergne gravity anomalies	26
Figure 3.5 : Simple Bouguer gravity anomalies	27
Figure 3.6 : Gridded simple Bouguer gravity anomalies.....	27
Figure 3.7 : Gridded values of Auvergne surface gravity anomalies	28
Figure 3.8 : Gridded values of Auvergne surface gravity disturbance.....	29
Figure 3.9 : Gravity observations in discrete form.....	30
Figure 3.10 : Gravity observations partitioned according to Voronoi cell structures.....	30
Figure 3.11 : Data borders which residual Voronoi polygons are selected ...	31
Figure 3.12 : Data borders which residual Voronoi polygons are removed..	31
Figure 3.13 : Illustration of the height systems	32
Figure 3.14 : Auvergne topography	33
Figure 4.1 : Near zone geoid contribution computed by using grid-wise evaluation of LSMHA	37
Figure 4.2 : Far zone geoid contribution computed by using grid-wise evaluation of LSMHA	37
Figure 4.3 : Combined atmospheric correction on geoid model com- puted by using grid-wise evaluation of LSMHA.....	38
Figure 4.4 : Combined topographic correction on geoid model com- puted by using grid-wise evaluation of LSMHA.....	38
Figure 4.5 : $\delta N_{DWC}^{(1)}(P)$ effect on geoid model computed by using grid-wise evaluation of LSMHA.....	39
Figure 4.6 : $\delta N_{DWC}^{L(1),far}(P)$ effect on geoid model computed by using grid-wise evaluation of LSMHA.....	39
Figure 4.7 : $\delta N_{DWC}^{L(2)}(P)$ effect on geoid model computed by using grid-wise evaluation of LSMHA.....	40
Figure 4.8 : Combined Ellipsoidal effect on geoid model computed by using grid-wise evaluation of LSMHA.....	40
Figure 4.9 : Final geoid from grid-wise evaluation of LSMHA	43
Figure 4.10 : Final geoid from grid-wise evaluation of LSMHA	43

Figure 4.11: Final geoid from point-wise evaluation of LSMHA 44
Figure 4.12: Final geoid from point-wise evaluation of LSMSA..... 44
Figure 5.1 : Limitation on the integration area 46
Figure 5.2 : 3D matrix..... 47



GEOID MODELING BY THE LEAST SQUARES MODIFIED HOTINE FORMULA USING VORONOI CELL STRUCTURES

SUMMARY

Increasing use of satellite based positioning techniques in combination with geoid based vertical datum definition for height determination motivates studies on precise geoid modeling. This is supported by the developments in spatial data acquisition techniques and progress in computational methodologies that facilitate computations of accurate and high resolution geoid models. Even though several recent dedicated gravimetric satellite missions (such as GRACE and GOCE) have enhanced accuracy and spatial resolution global geopotential models (GGMs), however, the spatial resolution of GGMs remains still insufficient for many applications. The benefits of these improvements at the long and middle wavelengths of the gravity field signal to the regional geoid mapping become more accurate.

This study provides the methodological characteristics of the gravity field modeling and shows a mathematical comparison among the frequently applied methodologies. In spherical approximation, geoid undulation can be determined by using a modified Stokes formula, which combines local terrestrial gravity anomalies and the GGM-derived long wavelength component in a truncated Stokes's integral (LSMSA). As an alternative, this study proposes the Least Squares Modified Hotine Formula with Additive Corrections (LSMHA) for geoid modeling. Once the approximate geoid with the Least Squares Modified Hotine Function is computed, the additive corrections should be implemented to the model. The present study tests the method by conducting an experimental geoid modeling in Auvergne area of France (43N and 49N latitudes, -1E and 7E longitudes). The GOCO05c geopotential model, digital terrain model data (grid form with 0.005° spacing), homogeneously distributed dense point gravity data and GNSS/leveling data are employed in the computations.

The Hotine function requires the use of gravity disturbances instead of anomalies. Gravity disturbance is a function of GNSS-derived ellipsoidal heights. Therefore the Hotine approach can be considered as a more practical approach in comparison with Stokes.

Usually, uniform grid of gravity quantities is needed as an input for Stokesian/Hotine's integration. However, since unsuitable gridding methods may produce false or spurious data that might lead to an inaccurate geoid, this study attempts to avoid conventionally gridded gravity data as an input to geoid modeling. Instead, the gravity data of the target area is partitioned into convex and adjacent polygons; each holds the original values of the

gravity disturbances. Within the integration area, the polygonal figures in Voronoi cell structures are used since the algorithm enables to preserve the actual characteristics of the observed gravity signal content. The resulting geoid models are assessed by the GNSS/leveling data and also compared to traditional geoid modeling approaches. Numerical results are provided in the conclusions of the study.



VORONOİ HÜCRE YAPILARI ARACILIĞIYLA HOTİNE İNTEGRALİNİN EN KÜÇÜK KARELER MODİFİKASYONU İLE GEOİT BELİRLEME

ÖZET

Günümüzde yüksek doğruluklu üç boyutlu konum bilgisine duyulan ihtiyaç oldukça artmış ve gelecekte de artmaya devam edeceği öngörülmektedir. Yüksek doğruluklu enlem ve boylam bilgisi Küresel Uydu Navigasyon Sistemleri (GNSS) kullanılarak hesaplanabilirken, uydu bazlı konumlama tekniklerinden elde edilen yükseklik bilgisi elipsoid referanslı bir yüzeyi ifade etmektedir. Jeodezik altyapıya referans teşkil eden ortometrik yükseklikler (ortalama deniz yüzeyi referanslı) ise nivelman yöntemi ile belirlenebilmekte ancak bu yöntem hem zaman hem de finansal açıdan istenilen verimi sunamamaktadır. Aynı zamanda nivelman yönteminde ölçme hatalarının kümülatif olarak takip eden ölçmeyi etkilemesinden dolayı istenilen doğruluk elde edilememektedir. Klasik geometrik ve trigonometrik nivelmanın aksine prezisyonlu geometrik nivelman ölçme doğruluğu açısından daha doğru sonuçlar verse de uygulaması daha zor ve zaman alan bir yöntemdir.

Yer yuvarının kütesinden kaynaklı çekim potansiyeli ve sahip olduğu açısız hızdan kaynaklı merkezkaç potansiyelinin bileşkesi gravite potansiyeli olarak ifade edilir. Gravite potansiyeli eşit olan noktaların oluşturduğu yüzeyler eşpotansiyel, diğer bir ifade ile nivo yüzeyleri olarak adlandırılır. Geoit fiziksel anlamda ortalama deniz yüzeyine yakınsayan ve karaların altından devam ettiği varsayılan özel bir eşpotansiyel yüzeydir. Bu bağlamda geoit belirleme problemi, bir gravite alanı modellemesi işlemi olarak ifade edilebilir. Gravite alanı modellemesi matematiksel olarak belli sınır koşuluna bağlı olarak ilgili parametrelerin diferansiyel denklem sisteminde çözümünü, yani literatürde belirtildiği üzere jeodezik bir sınır değer problemini ifade etmektedir.

GNSS yöntemiyle bulunan elipsoidal yükseklik ile geoit yükseklikleri kullanılarak pratik uygulamalarda ihtiyaç duyulan ortometrik yükseklik bilgisi elde edilebilmektedir. Geoit yüksekliğinin hesaplanması ise yaygın olarak gravimetrik yöntemlerle gerçekleştirilmektedir. Bu bağlamda uydu bazlı konumlama tekniklerinin de gelişmesiyle yükseklik sistemi belirleme amaçlı geoit referanslı düşey datum tanımlamaları günümüzde önem kazanmıştır.

Yersel gravite verilerinin doğruluğunun artması ve hesap yöntemlerindeki modifikasyonlarla yüksek doğruluklu ve yüksek çözünürlüklü gravimetrik geoit modellerinin hesaplanması kolaylaşmıştır. Uydu gravite misyonlarındaki gelişmeler (GRACE, GOCE), global jeopotansiyel modellerdeki (GGM) doğruluk ve mekansal çözünürlüğü arttırmış olsa da elde edilen sonuçlar günümüz ihtiyaçlarını tam anlamıyla karşılayamamaktadır. Bu amaçla yeni metodolojiler test edilmekte ve uygulamaya konulmaktadır. Yer yuvarı

üzerinde geoid yüksekliği hesaplanacak olan bölgedeki topografik yapı, gravite gözlemlerinin dağılımı ve doğruluğu, global jeopotansiyel modelin o bölgedeki performansı geoidin sonuç doğruluğunu etkileyeceğinden bu faktörler göz önüne alınarak uygun geoid modelleme yöntemi irdelenmelidir. Günümüzde En Küçük Kareler Kolokasyonu, Stokes/Hotine İntegral Yaklaşımı, Remove-Compute-Restore Tekniği ve Stokes-Helmert Metodu gibi yöntemler geoid belirleme amaçlı kullanılmaktadır.

Bu çalışma bölgesel geoid belirleme amacıyla sıklıkla kullanılan yöntemleri özetle incelemekte ve Hotine İntegralinin En Küçük Kareler Modifikasyonu ile bölgesel geoid belirleme tekniğinin teorisini ortaya koymaktadır. Hem Stokes hem de Hotine integralleri yardımıyla geoid belirlenirken; hesap yüzeyi bir küredir ve küre üzerinde homejen dağılımlı yersel gravite gözlemleri vardır kabul edilir. Ancak pratikte böyle bir imkan olmadığı için geoid yüksekliği belirlenecek bölgede bir sınırlandırma yapılır ki bu durum kesme hatasını beraberinde getirmektedir. Kesme hatasını elimine etmek adına Stokes/Hotine integralleri en küçük kareler yöntemi ile modifiye edilmektedir. En küçük kareler modifikasyonu temelde yersel gravite verisi ve GGM'lerden elde edilen parametrelerle hesaplanan gravite anomali veya bozukluklarının integrasyona hangi oranda katılacağını ifade eden modifikasyon parametrelerini sağlamaktadır. Yersel gravite verisi kullanılarak geoid modelinin kısa ve orta dalga boylu bileşenleri hesaplanırken, GGMlerden hesaplanan gravite ürünleriyle uzun dalga boylu geoid bileşeni bulunabilir. Yersel gravite verisi kullanılarak hesaplanan geoid bileşeni "yakın alan bileşeni" olarak isimlendirilirken, GGM yardımıyla hesaplanan ikinci bileşen "uzak alan bileşeni" olarak isimlendirilmektedir. Geoidin yakın ve uzak alan bileşenleri kullanılarak "yaklaşık geoid" elde edilebilmektedir. Hesap yüzeyinin integrasyonun başlangıcında küre olarak kabul edilmesi ve bu varsayımına ek olarak üzerinde topografik bir kütlelen olmadığı düşünülerek işlem yapılmasından kaynaklı, yaklaşık geoid hesabı, ek düzeltmeler ile iyileştirilmelidir. Bu bağlamda topografik, aşağıya uzanım, atmosferik ve elipsoidal düzeltmeler uygulanarak final geoidine ulaşılmalıdır.

Hotine Fonksiyonunun En Küçük Kareler Modifikasyonu (LSMHA), Stokes Fonksiyonunun En Küçük Kareler Modifikasyonundan (LSMSA) farklı olarak gravite anomalisi yerine gravite bozukluğu değerini kullanmaktadır. Günümüzde integral yöntemiyle geoid belirleme çalışmalarında yaygın olarak gravite anomalisi ile LSMSA yöntemi kullanılmaktadır. Ancak gravite bozukluğunun GNSS türevli elipsoidal yükseklikler kullanılarak direkt bir şekilde hesaplanabilmesiyle bu eğilimin değişebileceği düşünülmektedir. Nitekim bu amaçla LSMHA ve LSMSA metodlarının uygulanması ve kıyaslanması bu çalışma dahilinde yapılmıştır. Çalışma, Fransa'nın Auvergne bölgesinde (43N ve 49N enlemleri, -1E ve 7E boylamları arasında) gerçekleştirilen bir deneysel geoid modeli ile desteklenmektedir. Hesaplamalarda GOCO05C global geopotential modeli (360 °lik açılım), sayısal arazi modeli verileri (0.005° aralıklı grid formunda), homojen olarak dağılmış yoğun nokta gravite verileri ve validasyon amaçlı GNSS/nivelman verileri kullanılmıştır.

Genellikle Stokes / Hotine integrali için eş boyutlu homojen grid veri kullanılmaktadır. Bununla birlikte, uygun olmayan gridleme yöntemleri

yanlıř bir geoit modeline sebebiyet verebilecek veriler üretebileceđi için, bu çalıřma, geoit modelleme iřleminde geleneksel grid gravite verilerinin kullanımının önüne geçmeye çalıřmaktadır. Grid veri ve nokta veri kullanımının farklarını yansıtmak adına Auvergne bölgesinde iki yöntemle de geoit modeli hesaplanmış, yöntemler arasındaki farklar irdelenmiş ve sonuçlar ifade edilmiştir. Noktasal veri ile hesap yapabilmek adına her bir yersel gravite noktası, noktayı temsil edecek Voronoi alanları ile çevrelenmiştir. Her bir veri noktasını çevreleyen Voronoi alanları o noktayı çevreleyen diđer veri noktaları arasındaki uzaklıđın yarısına tekabül eden dönüm noktalarının birleřtirilmesi ile elde edilmektedir. Bu çalıřmada Voronoi alanları, harici bir yazılım aracılıđıyla oluşturulmuş, veri sınırlarında ortaya çıkan artık deđerler manuel olarak elimine edilmiştir. Voronoi alanları kullanılarak hesap yapılan alandaki gravite anomalisi veya gravite bozukluđu deđerleri gridleme iřlemindeki interpolasyondan kaynaklı hataları içermemekte, gravite sinyalinin olduđu gibi yansıtmaktadır. Bu deđerler ile yapılan hesaplamaların sonucunda veride öncelikli bir filtreleme iřleminin yapılması gerektiđi sonucuna varıldıysa da bu husus çalıřmanın odađı dıřında yer almaktadır.

Bu tez kapsamında, LSMHA ve LSMSA yöntemleri için hem grid veri hem de noktasal veri ile ortak olarak çalıřabilecek bir geoit modelleme algoritması oluşturulmuřtur. Hesaplanan geoit modelleri Auvergne veri seti ile birlikte sunulan 75 adet noktadan oluřan GNSS/nivelman gözlemleri yardımıyla valide edilmiş ve sonuçlar kıyaslanmıştır. 4 parametrelili Helmert benzerlik dönüřümü kullanılarak yapılan dengeleme iřlemi ile modellenen gravimetrik geoit ile GNSS/nivelmandan elde edilen geoit yüzeyleri arasındaki sistematik farklar giderilmiştir. Dengeleme öncesi ve sonrası model dođrulukları istatistiksel olarak ifade edilmiştir.

Geoit belirleme üzerine bahsi geçen yöntemlerin uygulanması esnasında karřılařılan yazılımsal ve donanımsal güçlüklerin giderilmesi adına kullanılan donanımda deđiřikliđe gidilmiş ve algoritmada performans geliştirme ihtiyacı dođmuřtur. Bu bağlamda yazılan kodlar aynı anda paralel iřlemcilerde kořturulabilecek řekilde optimize edilmiştir.

Yapılan analizlerin sonucunda, grid veri ile yapılan LSMSA ve LSMHA uygulamalarında yüksek dođruluk elde edilirken, nokta veri ile nispeden daha düşük bir dođruluđa ulařılmıştır. Uygulamalara yönelik sayısal analizler, tartıřma ve gelecek arařtırmalara yönelik fikir ve öneriler sonuç bölümünde sunulmuřtur.



1. INTRODUCTION

1.1 Background

Geoid is a special level surface consists of points having the same gravity potential and approximates to mean sea level. Due to the irregularities of the masses and the rotation of the Earth, geoid has a non-uniform shape. The shape is expressed as the geoid height (undulation) which is defined with respect to a reference ellipsoid and notated as N . Despite being a physical surface, geoid has a practical usage in geodetic infrastructure, as the reference surface of topographical heights and also used in geophysics and geodynamics to study the quantities related to deep Earth. As shown in Figure 1.1, when GNSS-derived ellipsoidal heights h and a reliable geoid model are available, one can determine the sea level referred (orthometric) height H by:

$$H = h - N \quad (1.1)$$

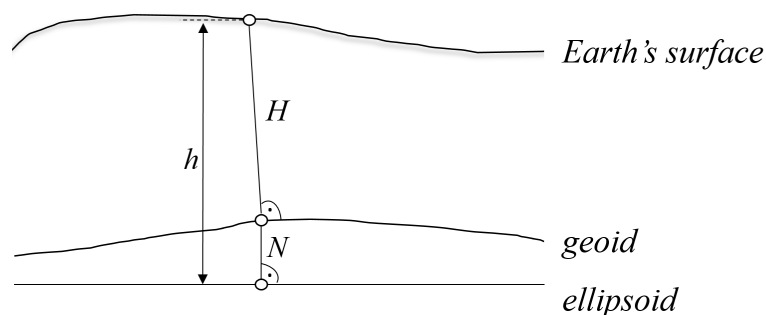


Figure 1.1 : Height reference surfaces

In terms of geodetic prospect, due to relatively higher time and money consumption and the cumulative error propagation of leveling procedure, geoid modeling is considered as a more efficient approach on vertical datum definition. In consideration of the recent studies, the accuracy of geoid highly depends on the data density and the data accuracy. Ågren and Sjöberg (2014) presents the gravity data requirements for 5 mm quasigeoid model in Swedish

and Nordic regions (under the context of this thesis only geoid model is examined however, the mentioned requirements can be considered valid for both quasigeoid and geoid models). It is also suggested to investigate Farahani et al. (2017) for a similar study conducted in Netherlands where the standard deviation of 1.5 mGal for the surface gravity anomaly and a data spacing of about 3.5 to 6.5 km are considered as sufficient for 5 mm quasigeoid model. Along with the data condition, the final accuracy of the geoid model is also dependent on the method used.

Methods used in gravity field modeling include Remove Compute Restore (RCR), Stokesian/Hotine Integration, Stokes/Helmert Method, and Least Squares Collocation (LSC) techniques. Each technique evaluates terrestrial gravity measurements, mostly gravity anomaly; derived from the observations. While LSC approach uses point-wise evaluation, the rest of the methods often use gridded gravity quantities. On the other hand, as it is previously investigated in Dos Santos and Escobar (2004), the gravity anomalies can be discretely used in Stokes Integral. The similar procedure can be applied for Hotine Integral using point-wise evaluation which constitutes the main focus of this thesis. As distinct from Stokesian integration, Hotine approach requires gravity disturbance values as the input.

The short wavelength/high frequency component of the geoid signal represents a rapidly changing surface while the long wavelength/low frequency component represents a relatively smoother surface. Global geopotential models (GGMs) obtained from space geodetic missions such as GRACE (Gravity Recovery and Climate Experiment) and GOCE (Gravity field and steady-state Ocean Circulation Explorer) offer global scale gravity quantities. Spherical harmonic expansion of GGM derived quantities are used to get a reference field for the local approximation of the geoid which represents the long wavelength part (Li, 2000). Geoid information of short/medium wavelengths is determined using terrestrial gravity observations were located in a cap of integration. While determination of the radius of the integration cap is highly dependent on the quality of the terrestrial data, the upper modification limit of the integration is related to the accuracy and the spatial

resolution of the GGM (Işık, 2016) and the compatibility of the model with the specific area to be modeled (see Section 4.1).

1.2 Purpose of the Study

The overall objective of this study is to compute a high resolution geoid model for Auvergne area, France. For this purpose, both Least Squares Modification of Stokes' (LSMS) and Least Squares Modification of Hotine's (LSHS) formulas are applied, and the results are given for different solutions by using biased, unbiased, and optimum type of modification parameters presented in Ellmann (2004) and Märdla et al. (2018).

The emphasis of the study is to compare the geoid modeling methods by Stokes/Hotine integral approach using point-wise and grid-wise gravity data. It is also aimed to introduce an applicable solution for singularity problem for discrete (point-wise) evaluation which will be investigated in Section 2.7.

1.3 Outline

The thesis constituted in six chapters. Chapter 1 indicates the statement of the problem in sense of the gravity field and the geoid. It gives a brief explanation of geoid accuracy and geoid components in accordance with the main objective of the study. Chapter 2 is meant as an overall investigation of the gravity related quantities, definitions of Earth's gravity field, and the fundamentals of physical geodesy. The theories behind the geoid modeling methods implied in this study are shown and the differences between those techniques are demonstrated. In Chapter 3, the data available in the study area is introduced. Chapter 4 comprises the numerical results of the methods those previously introduced in Chapter 2. Computational difficulties confronted during the study are explained in Chapter 5. Chapter 6 summarises the findings of the study and recommendations for future studies based on the results are presented in this section.

2. METHODOLOGY

2.1 Gravity Potential and Geoid

Gravity potential is the product of the gravitational potential and the centrifugal potential (Freedon et al., 2015). Gravitational potential of the Earth depends on the attraction of masses while the centrifugal potential is related to the rotation of the celestial body, the Earth in particular. Based on this definition a leveling surface can be described as a set of points consisting the same value of gravity potential. Among all leveling surfaces, Geoid as a special surface is introduced by Listing (1873).

As it introduced in Chapter 1, geoid is an equipotential surface shaped by the points with the same gravity potential values and it approximates the mean sea level. As a matter of fact, geoid is a physically defined surface with practical implementation that stands for the height N with respect to a global reference ellipsoid. Geoid determination is based on the Second Boundary Value Problem (Neumann's problem) or Third Boundary Value Problem (Robin's problem) that determines the disturbing potential on a surface, on which values functionally related to this disturbing potential exist (Bayoud and Sideris, 2003).

There are different methods to model the geoid. LSC method stated in Chapter 1, is a type of interpolation and/or prediction of stochastic variables, either within one type of observable or from the observations of one type to another (Sjöberg and Bagherbandi, 2017). RCR technique; as an alternative, even though is considered as a commonly used method, remains incapable since the assumptions in RCR technique (such as usage of Helmert's second method of condensation while elimination of topographic effect, ignoring the atmospheric correction, etc.) do not reflect the reality. In this context, KTH (Royal Institute of Technology) Method, first introduced by Sjöberg (1984), investigated in detail. The theory also called the Least Squares Modification of

Stokes Integral with Additive Corrections (LSMSA), applied to modify Stokes kernel to minimize the global mean square error of the resulting geoid model (see e.g. Ellmann (2001) and Ågren (2004)). The theory makes use of surface gravity anomaly instead of classical gravity anomaly on the geoid (see Section 2.3) to determine the approximate geoid and the additional corrections applied for the final geoid model. KTH method is applied in different regions having different characteristics of topography and showed convenient results (e.g. (Ellmann, 2004; Kiamehr, 2006; Ågren et al., 2009; Yildiz et al., 2012)).

For historical reasons, mostly gravity anomalies are evaluated for geoid modeling. Nowadays; however, since the ellipsoidal heights are directly available from GNSS, the gravity disturbance can be calculated accurately (see Section 2.4). Thus, one may expect that gravity disturbance will become more important than gravity anomaly in future (Hofmann-Wellenhof and Moritz, 2006).

Hotine integral for geoid determination, mentioned in Chapter 1, requires the integration of gravity disturbances (Hotine, 1969). For previous studies performed using Hotine integral, reader is referred to Zelin and Yecai (1991), Vanicek et al. (1992), Bayoud and Sideris (2003) etc. This thesis focuses on the Hotine adaptation of KTH method, so-called Least Squares Modification of Hotine's Integral with Additive Corrections (LSMHA) first presented by Mårdla et al. (2018). The novelty of this study is based on discrete data evaluation instead of using regular gravity grids as distinct from the former study.

2.2 Normal Gravity

The normal figure of the Earth is considered as a level ellipsoid due to the simplicity on computations. In theory, the gravity value on the level ellipsoid is regarded as the normal gravity (Hofmann-Wellenhof and Moritz, 2006).

The normal gravity γ_{Q_0} on a point Q_0 located at the ellipsoidal surface as shown in Figure 2.1 is given by the well-known formula of Somigliana:

$$\gamma_{Q_0} = \frac{a\gamma_a \cos^2(\varphi) + b\gamma_b \sin^2(\varphi)}{\sqrt{a^2 \cos^2(\varphi) + b^2 \sin^2(\varphi)}} \quad (2.1)$$

where a and b are respectively the semi-major and semi-minor axes of the ellipsoid, γ_a and γ_b are the normal gravity at the equator and the poles, and φ is the latitude of the point corresponds to Q_0 on ellipsoid.

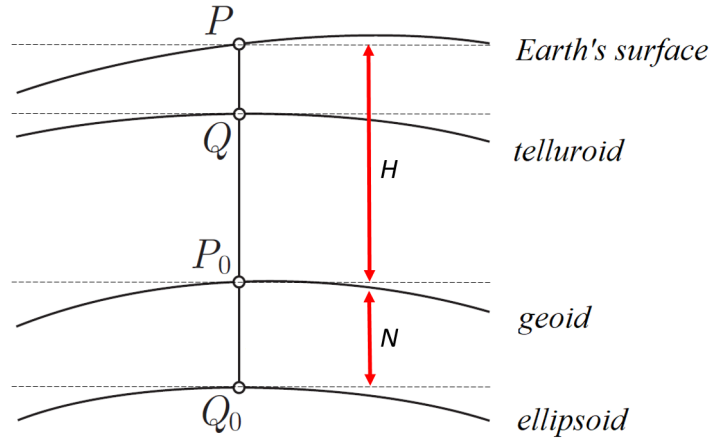


Figure 2.1 : Illustration of the relevant surfaces (Hofmann-Wellenhof and Moritz, 2006)

2.3 Gravity Anomaly

Gravity anomaly vector is the difference between the actual gravity vector on the geoid \vec{g}_{P_0} and the normal gravity vector on the reference ellipsoid $\vec{\gamma}_{Q_0}$ as shown in Figure 2.1. The difference in magnitude is defined as the classical gravity anomaly Δg_0 (Hofmann-Wellenhof and Moritz, 2006):

$$\Delta g_0 = g_{P_0} - \gamma_{Q_0} \quad (2.2)$$

Analogously the modern gravity anomaly Δg according to Molodensky's theory (also called surface gravity anomaly) is defined as (Molodensky, 1962; Hofmann-Wellenhof and Moritz, 2006):

$$\Delta g = g_P - \gamma_Q \quad (2.3)$$

as it can be seen in the Figure 2.1, P is the point at the Earth's surface and γ_Q is the normal gravity at the same ellipsoidal longitude and latitude reduced

to telluroid (a spheropotential surface where $U = W_P = const$, see Figure 3.13) (Hofmann-Wellenhof and Moritz, 2006).

For many purposes such as interpolating the surface gravity values, a functional of the gravitational potential which does not contain the effect of the topographic masses above the geoid is needed (Barthelmes, 2009). The former leads to the simple Bouguer gravity anomaly Δg^{SBA} calculated as (Heiskanen and Moritz, 1967):

$$\Delta g^{SBA} = g_P - \left(\frac{\partial g_P}{\partial H}\right)^B H - \gamma_{Q_0} \quad (2.4)$$

where H is the orthometric height of the point located at the Earth's surface and

$$\left(\frac{\partial g_P}{\partial H}\right)^B = -0.1967 \text{ mGal/m} \quad (2.5)$$

is the Bouguer gradient assuming the crustal density ρ equals to 2.67 g/cm^3 (Vanicek and Krakiwsky, 2015).

Due to the rapid change on the topography, the reduced anomaly quantities may not be convenient hence a smoother gravity field might be required for gridding procedure. In this case terrain corrected Bouguer anomalies also known as complete Bouguer anomalies must be evaluated from the following formula (Märdla et al., 2017):

$$\Delta g^{CBA} = \Delta g^{SBA} + \delta g^{TC} \quad (2.6)$$

where δg^{TC} is the terrain correction (Heiskanen and Moritz, 1967).

2.4 Gravity Disturbance

Gravity disturbance δg as another quantity of the gravity field can be obtained by using GNSS derived heights. δg on a point P located at the Earth's surface is expressed as (Heiskanen and Moritz, 1967):

$$\delta g_P = g_P - \gamma_P \quad (2.7)$$

where γ_P is the normal gravity on topography and calculated as:

$$\gamma_P = \gamma_{Q_0} - 0.3086h \quad (2.8)$$

where the second part from the right side of the equation is the terrain correction while h is the height above the ellipsoid.

2.5 Geoid Modeling with KTH Method

The difference between the actual gravity potential on geoid and the normal gravity potential on ellipsoid is denoted as disturbing potential; T (Hofmann-Wellenhof and Moritz, 2006). According to Stokes (1849), T can be computed as:

$$T = \frac{R}{4\pi} \iint_{\sigma} S(\psi) \Delta g d\sigma \quad (2.9)$$

The relationship between the geoid height and the disturbing potential is given by the well-known formula of physical geodesy by Bruns (1878) as:

$$N = \frac{T}{\gamma} \quad (2.10)$$

Accordingly, the geoid height can be expressed using Stokes equation as:

$$N = \frac{R}{4\pi\gamma} \iint_{\sigma} S(\psi) \Delta g d\sigma \quad (2.11)$$

Geoid determination with original Stokes formula as expressed in Eq. 2.11 requires global coverage of gravity anomalies. However, since a homogeneous, dense gravity data cannot be obtained in global scale, the integration is limited in a circle of radius ψ_0 . Due to the truncation error, original Stokes function should be modified by sets of stochastic or deterministic modification parameters; presented as s_n and b_n (Ellmann, 2005).

KTH (Royal Institute of Technology) method summarized by Sjöberg (2003b) states for the Least Squares Modification of Stokes's Formula with Additive Corrections (LSMSA). In order to perform the KTH method, the surface gravity anomalies within a predefined integration cap are directly used to calculate the short and medium wavelength components of the geoid (near zone geoid). Long wavelength component (far zone geoid) stems from the evaluation of the spherical harmonic function of the gravity anomaly calculated in a proper degree of modification. The geoid estimator \hat{N} is acquired by applying the

additive corrections and represented as:

$$\hat{N} = \tilde{N} + \delta N_{COMB} + \delta N_{DWC} + \delta N_{ATM} + \delta N_{ELL} \quad (2.12)$$

\tilde{N} stands for the approximate geoid, δN_{COMB} represents the combined topographic effect (Sjöberg, 1995, 2000), while δN_{DWC} is the combined downward continuation effect (Sjöberg, 2003c). δN_{ATM} stands for the combined atmospheric effect introduced in Sjöberg (1999) and Sjöberg (2001). Lastly, δN_{ELL} presents the combined ellipsoidal effect (Sjöberg, 2003a, 2004).

Approximate geoid \tilde{N} composes of two parts:

$$\tilde{N} = N_{near} + N_{far} \quad (2.13)$$

In order to calculate \tilde{N} in a truncated cap σ_0 , Eq. 2.13 is expanded as (Sjöberg, 2003b):

$$\tilde{N} = \frac{R}{4\pi\gamma} \iint_{\sigma_0} S^L(\psi) \Delta g d\sigma + \frac{R}{2\gamma} \sum_{n=2}^M b_n \Delta g_n \quad (2.14)$$

where R is the mean Earth radius

γ is normal gravity at the ellipsoid

$S^L(\psi)$ is modified Stokes function

Δg are surface gravity anomalies

$d\sigma$ are surface elements

b_n are the modification parameters

Δg_n are the spherical harmonic representation of the gravity anomaly

L is the selected maximum degree of modification and M is the spherical harmonic degree up to which GGM is used.

Since the main emphasis of this study is to implement LSMHA (Hotine) procedure and both Stokes/Hotine functions show resemblance (Heiskanen and Moritz, 1967), the detailed explanations of components mentioned above

will be represented for Least Squares Modification of Hotine's Function with Additive Corrections in Section 2.6 and 2.6.1. The summary of the comparison between Stokes and Hotine procedures is given in Table 2.1, Table 2.2, and Table 2.3.

2.6 Least Squares Modification of Hotine's Function

At the present time, the vertical component of position can be obtained by GNSS with less than 1 cm accuracy. As it is stated in previous sections, one can determine gravity disturbance accurately with ellipsoidal heights. Gravity field of the Earth can be modeled by using gravity disturbance via Hotine integral. The general form of geoid undulation using Hotine integral is given as (Hotine, 1969):

$$N = \frac{R}{4\pi\gamma} \iint_{\sigma} H(\psi) \delta g d\sigma \quad (2.15)$$

R is the mean Earth radius. γ equals to the normal gravity on the reference ellipsoid, σ is the unit sphere, $H(\psi)$ is the Hotine function, δg is the gravity disturbance, and $d\sigma$ is the elemental area of each observation point.

The original form of Hotine function is given as (Hotine, 1969):

$$H(\psi) = \frac{1}{\sin(\psi/2)} - \log\left(1 + \frac{1}{\sin(\psi/2)}\right) \quad (2.16)$$

As already expressed in Section 2.5, due to the lack of global coverage of gravity data, the integration should be limited in a truncated cap using a set of modification parameters. In order to do so, Eq. 2.15 is rewritten as below while near zone and the far zone contributions are taken into account separately (Märdla et al., 2018):

$$\tilde{N} = \frac{R}{4\pi\gamma} \iint_{\sigma_0} H^L(\psi) \delta g d\sigma + \frac{R}{2\gamma} \sum_{n=0}^M b_n \delta g_n \quad (2.17)$$

where $H^L(\psi)$ is the modified Hotine function, δg is the surface gravity disturbance, b_n are the modification parameters calculated for LSMHA, δg_n are the Laplace harmonics of gravity disturbance and the rest of the terms are identical with the terms explained in Section 2.5. Note that n in the second part of the formula starts from 0 instead of 2 compared to Stokes counterpart.

The modified Hotine function $H^L(\psi)$ can be computed as (Märdla et al., 2018):

$$H^L(\psi) = H(\psi) - \sum_{n=0}^L \frac{2n+1}{2} s_n P_n(\cos(\psi)) \quad (2.18)$$

$P_n(\cos(\psi))$ are the un-normalized Legendre polynomials of $\cos(\psi)$ where ψ are the spherical distances calculated from computation point to each integration point.

The spherical harmonic representation of the gravity disturbance is given as (Heiskanen and Moritz, 1967, Eq. 2-153):

$$\delta g_n = \frac{GM}{a^2} \left(\frac{a}{r}\right)^{n+2} (n+1) \sum_{m=0}^n \{ \overline{\Delta C}_{nm} \cos m\lambda + \overline{S}_{nm} \sin m\lambda \} \overline{P}_{nm}(\sin \phi) \quad (2.19)$$

where \overline{P}_{nm} are fully normalized Legendre polynomials, r , λ , and ϕ are geocentric radius, longitude, and geocentric latitude of computation point respectively. \overline{C}_{nm} and \overline{S}_{nm} are fully normalized spherical harmonic coefficients and $\overline{\Delta C}_{nm}$ is calculated as (Ellmann, 2001):

$$\overline{\Delta C}_{nm} = \overline{C}_{nm}^W - \overline{C}_{nm}^U \quad (2.20)$$

where \overline{C}_{nm}^W is the related degree and order \overline{C}_{nm} coefficients obtained by the GGM and \overline{C}_{nm}^U represents the fully normalized even zonal harmonics of normal potential.

The modification parameters b_n are calculated for biased, unbiased, and optimum solutions as (Ellmann, 2005):

$$\begin{aligned} \text{biased} : \quad b_n &= s_n \\ \text{unbiased} : \quad b_n &= s_n + Q_n^L \\ \text{optimum} : \quad b_n &= \frac{(s_n + Q_n^L)c_n^2}{(c_n^2 + dc_n^2)} \end{aligned} \quad (2.21)$$

where s_n are the modification parameters, Q_n^L are the modified truncation coefficients, c_n^2 are the gravity signal degree variances, and dc_n^2 are the GGM error degree variances.

The modified truncation coefficients $Q_n^L(\psi_0)$ for the spherical distance of ψ_0 are computed as (Märdla et al., 2018):

$$Q_n^L(\psi_0) = Q_n(\psi_0) - \sum_{k=0}^L \frac{2k+1}{2} R_{nk} s_k \quad (2.22)$$

$Q_n(\psi_0)$ are the truncation coefficients by Jekeli (1979). R_{nk} are calculated according to Paul (1973). s_k are the modification parameters (same as s_n in Eq. 2.18)

Apart from KTH procedure, the spectral factor used in the computation of s_n parameters in Stokes modification; $1/(n - 1)$ is replaced by $1/(n + 1)$ for Hotine approach. Another difference is that the truncation coefficient $Q_n(\psi_0)$ from Paul (1973) is used for Stokesian integration.

In this thesis, modification parameters s_n and b_n are calculated using a software provided by Prof. Dr. Artu Ellmann for both Stokes and Hotine procedures.

2.6.1 Additive corrections

There are a number of assumptions while implementing Stokes/Hotine integrals for geoid modeling:

- The integration area is a sphere
- There is homogeneous data along the whole sphere of integration
- There are no topographic masses outside of the sphere of integration

The second assumption indicated above carried out by implementing modification parameters to the integral (see Section 2.5 and 2.6). Yet, a number of corrections should be performed due to the first and the third presumptions. After the integration, indirect effects are applied to the potential for restoration of masses as well as for corrections to the potential on the reference ellipsoid (Sjöberg and Bagherbandi, 2017).

Additive corrections for least squares modification of Hotine function shows resemblance with the corrections in the least squares modification of Stokes function. Sequent section presents the corrections needed to be implemented on LSMH and shows the comparisons between LSMH and LSMS approaches.

2.6.1.1 Combined topographic correction

In traditional methods, the potential of gravity anomaly or disturbance are located on the geoid while implementing Stokes/Hotine integral. Since

there should be no topographic masses outside of the integration sphere, the topographic signal on gravity must be removed (by any method) and should be restored once the integration is implemented; however, due to the incomplete downward continuation, this technique leads to an error (Sjöberg, 2018). Finally, after the adoption of surface gravity anomaly or disturbances, the combined topographic correction can be carried out by (Sjöberg, 2018):

$$\delta N_{COMB} = -\frac{2\pi G\rho}{\gamma} \left(\widetilde{H}^2 + \frac{2\widetilde{H}^3}{3R} \right) \quad (2.23)$$

where G is the Newton's gravitational constant, ρ is the topographic density, and \widetilde{H}^v is the v th power of the Laplace surface harmonics of the topographic height with first and second-degree terms excluded (see Eq. 3.5). However, in this study; since the orthometric height of each integration point is provided by the Auvergne dataset (see Section 3.1), the observed values are directly used instead of the Laplace surface harmonics of the topographic heights.

2.6.1.2 Combined downward continuation correction

Combined downward continuation correction can be calculated as:

$$\delta N_{DWC} = \delta N_{DWC}^{(1)}(P) + \delta N_{DWC}^{L(1),far}(P) + \delta N_{DWC}^{L(2)}(P) \quad (2.24)$$

$\delta N_{DWC}^{(1)}(P)$ is the first component of downward continuation effect (Märdla et al., 2018):

$$\delta N_{DWC}^{(1)}(P) = \frac{\delta g(P)}{\gamma} H_P + \frac{\zeta_P^0}{r_P} H_P - \frac{1}{2\gamma} \frac{\partial \delta g}{\partial r} \Big|_P H_P^2 \quad (2.25)$$

where ζ_P^0 is the approximate value of height anomaly and as suggested in Ågren (2004):

$$\zeta_P^0 \approx \widetilde{N} \quad (2.26)$$

$\frac{\partial \delta g}{\partial r} \Big|_P$ is the vertical gradient of gravity disturbance as in Heiskanen and Moritz (1967). It should be noted that the second term of the equation should be multiplied with 3 in LSMSA compared to Hotine counterpart.

$\delta N_{DWC}^{L(1),far}(P)$ is the term for far component of downward continuation correction and expressed as follow (Märdla et al., 2018):

$$\delta N_{DWC}^{L(1),far}(P) = \frac{R}{2\gamma} \sum_{n=0}^M (s_n + Q_n^L) \left[\left(\frac{R}{r_P} \right)^{n+2} - 1 \right] \delta g_n(P) \quad (2.27)$$

where $\delta g_n(P)$ are the gravity disturbance of computation point from spherical harmonics calculated as in Eq. 2.19.

Finally, the terrain downward continuation effect (Märdla et al., 2018):

$$\delta N_{DWC}^{L(2)}(P) = \frac{R}{4\pi\gamma} \iint_{\sigma_0} H^L(\psi) \left(\frac{\partial \delta g}{\partial r} \Big|_Q (H_P - H_Q) \right) d\sigma_Q \quad (2.28)$$

Notice that the gravity quantities used in the calculations above are the disturbance values instead of anomalies compared to the Stokes counterpart.

2.6.1.3 Combined atmospheric correction

Considering the third assumption introduced in section 2.6.1, the effect of the atmospheric masses should be taking into account as (Märdla et al., 2018):

$$\begin{aligned} \delta N_{ATM}(P) = & -\frac{2\pi R G \rho_A}{\gamma} \sum_{n=0}^M \left(\frac{2}{n+1} - s_n - Q_n^L \right) H_n(P) \\ & - \frac{2\pi R G \rho_A}{\gamma} \sum_{n=M+1}^{\infty} \left(\frac{2}{n+1} - \frac{n+2}{2n+1} Q_n^L \right) H_n(P) \end{aligned} \quad (2.29)$$

where G is the Newton's gravitational constant, ρ_A is the atmospheric density at sea level, and H_n are the Laplace surface harmonics of the topographic height (Eq. 3.5).

2.6.1.4 Combined ellipsoidal correction

As introduced in section 2.6.1, Stokes/Hotine integrals are implemented using spherical coordinates. Therefore, the combined ellipsoidal correction should be calculated as (Märdla et al., 2018):

$$\delta N_{ELL}(P) = \frac{R}{2\gamma} \sum_{n=0}^{\infty} \left(\frac{2}{n+1} - s_n - Q_n^L \right) \left(\frac{a-R}{R} \delta g_n(P) + \frac{a}{R} \delta g_n^e \right) \quad (2.30)$$

where $\delta g_n(P)$ are the gravity disturbance of computation point from spherical harmonics calculated as in Eq. 2.19 and δg_n^e are the Laplace harmonics of

the ellipsoidal correction to the gravity disturbance and presented as (Märdla et al., 2018):

$$\delta g_n^e = \frac{e^2 GM}{2a^2} \sum_{m=-n}^n \{ [3 - (n+4)F_{nm}]C_{nm} - (5-n)G_{nm}C_{n+2,m} - (3n+7)E_{nm}C_{n-2,m} \} Y_{nm}(P) \quad (2.31)$$

Y_{nm} are the fully normalized spherical harmonics, C_{nm} are the harmonic coefficients of the disturbing potential and E_{nm} , F_{nm} , and G_{nm} are the related coefficients for the ellipsoidal correction.

2.7 Singularity Problem

Hotine function (as well as Stokes function) introduced in Eq. 2.16 is equal to ∞ while $\psi = 0$. As shown in Figure 2.2 this effect has also an impact on the integration points which are located close to the computation point (see the sudden decrease where the spherical distances are close to zero) and called as singularity problem.

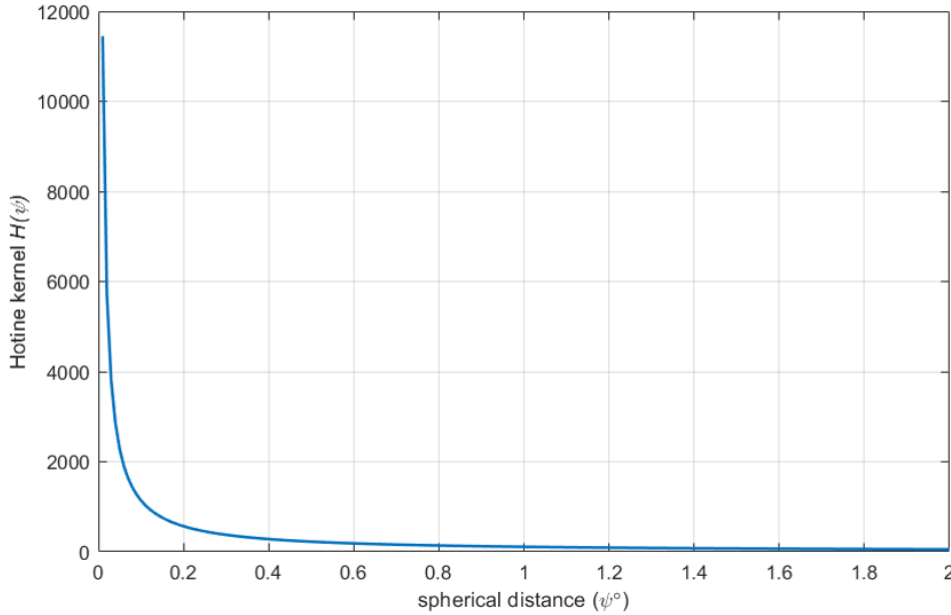


Figure 2.2 : Unmodified Hotine function for the spherical distances calculated in the truncation cap

In order to diminish the singularity effect, the near zone component of the geoid presented as the first part in Eq. 2.14 can be divided into two parts:

$$N_{near} = N_{outer} + N_{inner} \quad (2.32)$$

N_{outer} expresses the term where the infinity outcome is eliminated and N_{inner} is for the gravity anomaly/disturbance of the computation point taken into account separately.

In order to overcome the undesired effects of the singularity problem, different considerations on Eq. 2.32 can be followed (Section 2.7.1-2.7.2)

2.7.1 The elimination of singularity for grid-wise evaluation

According to Ellmann (2001), singularity eliminated near zone component of geoid for LSMSA (Stokes) is expressed as:

$$N_{near} = \frac{R}{4\pi\gamma} \iint_{\sigma_0} S^L(\psi)(\Delta g_Q - \Delta g_P)d\sigma + \frac{R}{2\gamma}\Delta g_P Q_{M0} \quad (2.33)$$

where Δg_Q is the gravity anomaly of the integration point located inside the truncation cap, Δg_P is the gravity anomaly of the computation point, and Q_{M0} is the zero order term of the modified truncation coefficient and calculated as (Ellmann, 2001):

$$Q_{M0} = Q_0 - \sum_{k=0}^M \frac{2k+1}{2} s_k R_{k0} \quad (2.34)$$

where s_k are the modification parameters, R_{k0} are from Paul (1973), and Q_0 represents the zero degree term of Paul (1973) coefficient introduced in Section 2.5 and computed as follow:

$$Q_0 = -4t + 5t^2 + 6t^3 - 7t^4 + (6t^2 - 6t^4) \log t(1+t) \quad (2.35)$$

where $t = \sin(\frac{\psi_0}{2})$ and ψ_0 is the radius of the integration cap.

In order to compute the singularity eliminated near zone geoid for LSMHA (Hotine) approach; modified Stokes function $S^L(\psi)$, gravity anomaly Δg , truncation coefficient Q_0 from Paul (1973) should be replaced by modified Hotine function $H^L(\psi)$, gravity disturbance δg , and truncation coefficient Q_0 from Jekeli (1979) respectively.

As an alternative, the undesired effects of singularity can be eliminated using (Vajda and Vaníček, 1998):

$$N_{near} = \frac{R}{4\pi\gamma} \iint_{\sigma_0} S^L(\psi)\Delta g_Q \cos(\varphi_Q)(\Delta\varphi)^2 + \frac{R}{\gamma} \sqrt{\frac{\cos(\varphi_P)}{\pi}} \Delta g_P \Delta\varphi \quad (2.36)$$

φ_P and φ_Q represent the geocentric latitude of the computation and the running points respectively. $\Delta\varphi$ is the size of the integration grid. As a matter of course, the last term of the first part of the equation; $(\Delta\varphi)^2$ denotes the elemental area, uniform for each grid. The rest of the terms are the same where explained in the previous sections. For LSMHA (Hotine) approach; $H^L(\psi)$ and δg are used similarly.

In this thesis, the latter approach expressed in Eq. 2.36 gave better results and so was used instead.

2.7.2 The elimination of singularity for point-wise evaluation

While conducting the point-wise evaluation, running points and computation points may not be overlapped. However as it is stated in Section 2.7, singularity is an effect not only related to the overlapped point, but also affected by the running points located closely to the computation point. In this study, in order to eliminate this effect for point-wise evaluation, Eq. 2.33 is modified as:

$$N_{near} = \frac{R}{4\pi\gamma} \iint_{\sigma_0} S^L(\psi)(\Delta g_Q - \Delta g_{P^*})d\sigma + \frac{R}{2\gamma} \Delta g_{P^*} Q_{M0} \quad (2.37)$$

As it can be seen, Δg_P is replaced by Δg_{P^*} for point-wise evaluation. In the present case Δg_{P^*} stands for the gravity anomaly of the running point which is closest to the computation point. The rest of the terms can be calculated as explained in the previous section.

Analogously, Eq. 2.36 for point-wise evaluation is replaced by:

$$N_{near} = \frac{R}{4\pi\gamma} \iint_{\sigma_0} S^L(\psi)\Delta g_Q \cos(\varphi_Q)d\sigma + \frac{R}{\gamma} \sqrt{\frac{\cos(\varphi_{P^*})}{\pi}} \Delta g_{P^*} \sqrt{d\sigma} \quad (2.38)$$

where φ_{P^*} and Δg_{P^*} are the geocentric latitude and gravity anomaly of the integration point which is the closest to the computation point. Apart from grid-wise evaluation explained in Section 2.7.1, $(\Delta\varphi)^2$ is replaced by $d\sigma$ which is the elemental area of each Voronoi polygon surrounds point P^* (see Section 3.1.2 for Voronoi polygons). For LSMHA (Hotine) approach; $H^L(\psi)$ and δg are used similarly.

Table 2.1 : Comparison of LSMSA (Stokes) and LSMHA (Hotine) methods

Stokes	Hotine
$N = \frac{R}{4\pi\gamma} \iint_{\sigma} S(\psi) \Delta g d\sigma$	$N = \frac{R}{4\pi\gamma} \iint_{\sigma} H(\psi) \delta g d\sigma$
$S(\psi) = \sum_{n=2}^{\infty} \frac{2n+1}{n-1} P_n(\cos(\psi))$	$H(\psi) = \sum_{n=0}^{\infty} \frac{2n+1}{n+1} P_n(\cos(\psi))$
$\tilde{N} = \frac{R}{4\pi\gamma} \iint_{\sigma_0} S^L(\psi) \Delta g d\sigma + \frac{R}{2\gamma} \sum_{n=2}^M b_n \Delta g_n$	$\tilde{N} = \frac{R}{4\pi\gamma} \iint_{\sigma_0} H^L(\psi) \delta g d\sigma + \frac{R}{2\gamma} \sum_{n=0}^M b_n \delta g_n$
$S^L(\psi) = S(\psi) - \sum_{n=2}^L \frac{2n+1}{2} s_n P_n(\cos(\psi))$	$H^L(\psi) = H(\psi) - \sum_{n=0}^L \frac{2n+1}{2} s_n P_n(\cos(\psi))$
$\Delta g_n = \frac{GM}{a^2} \left(\frac{a}{r}\right)^{n+2} (n-1) \times$ $\sum_{m=2}^n \{ \Delta C_{nm} \cos m\lambda + \bar{S}_{nm} \sin m\lambda \} \bar{P}_{nm}(\sin \phi)$	$\delta g_n = \frac{GM}{a^2} \left(\frac{a}{r}\right)^{n+2} (n+1) \times$ $\sum_{m=0}^n \{ \Delta C_{nm} \cos m\lambda + \bar{S}_{nm} \sin m\lambda \} \bar{P}_{nm}(\sin \phi)$
$Q_n^L(\psi_0) = Q_n(\psi_0) - \sum_{k=0}^L \frac{2k+1}{2} R_{nk} S_k$	
$Q_n(\psi_0) \text{ from Paul (1973)}$	$Q_n(\psi_0) \text{ from Jekeli (1979)}$
$R_{nk} \text{ from Paul (1973)}$	

Table 2.2 : Comparison of additive corrections for LSMSA (Stokes) and LSMHA (Hotine) methods

	Stokes	Hotine
\hat{N}		$\tilde{N} + \delta N_{\text{COMB}} + \delta N_{\text{DWC}} + \delta N_{\text{ATM}} + \delta N_{\text{ELL}}$
$\delta N_{\text{COMB}}(P)$		$-\frac{2\pi G\rho}{\gamma} \left(\tilde{H}^2 + \frac{2\tilde{H}^3}{3R} \right)$
$\delta N_{\text{DWC}}(P)$		$\delta N_{\text{DWC}}^{(1)}(P) + \delta N_{\text{DWC}}^{L(1),far}(P) + \delta N_{\text{DWC}}^{L(2)}(P)$
$\delta N_{\text{DWC}}^{(1)}(P)$	$\frac{\Delta g(P)}{\gamma} H_p + \frac{3\zeta_p^0}{r_p} H_p - \frac{1}{2\gamma} \frac{\partial \Delta g}{\partial r} \Big _p H_p^2$	$\frac{\delta g(P)}{\gamma} H_p + \frac{\zeta_p^0}{r_p} H_p - \frac{1}{2\gamma} \frac{\partial \delta g}{\partial r} \Big _p H_p^2$
$\delta N_{\text{DWC}}^{L(1),far}(P)$	$\frac{R}{2\gamma} \sum_{n=2}^M (s_n + Q_n^L) \left[\left(\frac{R}{r_p} \right)^{n+2} - 1 \right] \Delta g_n(P)$	$\frac{R}{2\gamma} \sum_{n=0}^M (s_n + Q_n^L) \left[\left(\frac{R}{r_p} \right)^{n+2} - 1 \right] \delta g_n(P)$
$\delta N_{\text{DWC}}^{L(2)}(P)$	$\frac{R}{4\pi\gamma} \iint_{\sigma_0} S^L(\psi) \left(\frac{\partial \Delta g}{\partial r} \Big _Q (H_p - H_Q) \right) d\sigma_Q$	$\frac{R}{4\pi\gamma} \iint_{\sigma_0} H^L(\psi) \left(\frac{\partial \delta g}{\partial r} \Big _Q (H_p - H_Q) \right) d\sigma_Q$

Table 2.3 : Comparison of additive corrections for LSMSA (Stokes) and LSMHA (Hotine) methods (continued)

	Stokes	Hotine
$\delta N_{ATM}(P)$	$-\frac{2\pi R G \rho_A}{\gamma} \sum_{n=2}^M \left(\frac{2}{n-1} - s_n - Q_n^L \right) H_n(P)$ $-\frac{2\pi R G \rho_A}{\gamma} \sum_{n=M+1}^{\infty} \left(\frac{2}{n-1} - \frac{n+2}{2n+1} Q_n^L \right) H_n(P)$	$-\frac{2\pi R G \rho_A}{\gamma} \sum_{n=0}^M \left(\frac{2}{n+1} - s_n - Q_n^L \right) H_n(P)$ $-\frac{2\pi R G \rho_A}{\gamma} \sum_{n=M+1}^{\infty} \left(\frac{2}{n+1} - \frac{n+2}{2n+1} Q_n^L \right) H_n(P)$
$\delta N_{ELL}(P)$	$\frac{R}{2\gamma} \sum_{n=2}^{\infty} \left(\frac{2}{n-1} - s_n - Q_n^L \right) \times$ $\left(\frac{a-R}{R} \Delta g_n(P) + \frac{a}{R} \delta g_n^e \right)$	$\frac{R}{2\gamma} \sum_{n=0}^{\infty} \left(\frac{2}{n+1} - s_n - Q_n^L \right) \times$ $\left(\frac{a-R}{R} \delta g_n(P) + \frac{a}{R} \delta g_n^e \right)$
δg_n^e	$\frac{e^2 GM}{2a^2} \sum_{m=-n}^n \{ [3 - (n+2)F_{nm}] C_{nm} - (n+1)G_{nm} C_{n-2,m}$ $-(n+7)E_{nm} C_{n+2,m} \} Y_{nm}(P)$	$\frac{e^2 GM}{2a^2} \sum_{m=-n}^n \{ [3 - (n+4)F_{nm}] C_{nm} - (5-n)G_{nm} C_{n+2,m}$ $-(3n+7)E_{nm} C_{n-2,m} \} Y_{nm}(P)$



3. DATA PREPARATION

Auvergne data set is provided by Institut Géographique National (IGN), France for testing the geoid modeling methods (Valty et al., 2012). So far different geoid computation methods are conducted in the area for scientific purposes such as Yildiz et al. (2012), Abbak and Ustun (2015), and Janák et al. (2017). The dataset includes a terrestrial gravity network, GNSS/leveling benchmarks, and a digital elevation model which will be explained in detail in Section 3.1, 3.2, and 3.3 respectively.

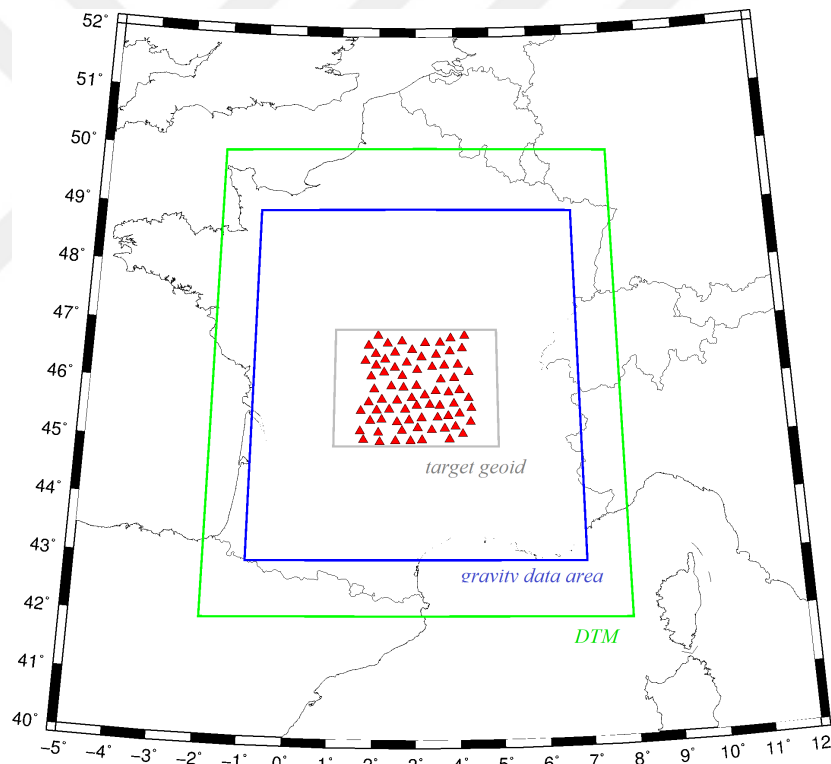


Figure 3.1 : Auvergne area

The outer frame in green shown in Figure 3.1 represents the area of digital terrain model while the inner box shown in blue includes terrestrial gravity observations. Red points in the innermost box represent the GNSS/leveling network. Target geoid location is shown as the grey box in the same figure.

3.1 Terrestrial Gravity Dataset

Terrestrial gravity dataset includes 244009 points of gravity measurements located in between $43 - 49N; -1 - (+7)E$ where shown in Figure 3.2. However, it is revealed that 83 of points are duplicated and supposed to be eliminated before the numerical evaluation. The mean density is 0.59 points per square kilometer while the standard deviation of the gravity anomaly is 20.70 mGal; mean, minimum, maximum values are 3.6 mGal, -127.47 mGal, and 177.82 mGal respectively according to Valtý et al. (2012). The accuracy of the gravity data is stated as $1 \sim 2$ mGal in the same study. Additionally; normal, orthometric, and ellipsoidal heights of each observation point are provided within the dataset.

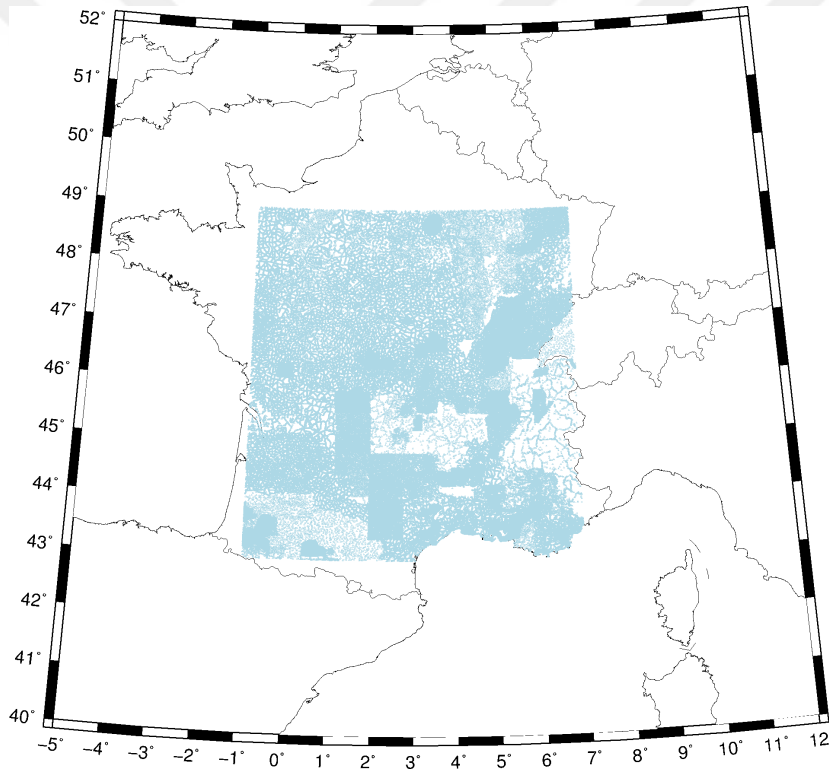


Figure 3.2 : Auvergne terrestrial gravity network

As it is introduced in Section 2.1, discrete data is directly used for geoid computations for point-wise evaluation as similarly has already been conducted by Dos Santos and Escobar (2004). In general, the technique used in this study to calculate the elemental area is to surround each data point with the most representative polygons by use of Voronoi diagrams will be explained in Section 3.1.2.

3.1.1 Input gravity quantities

Gravity disturbance used in point-wise integration of LSMHA (see Figure 3.3) is directly calculated from the dataset as (also shown in Section 2.4):

$$\delta g = g_P - \gamma_P \quad (3.1)$$

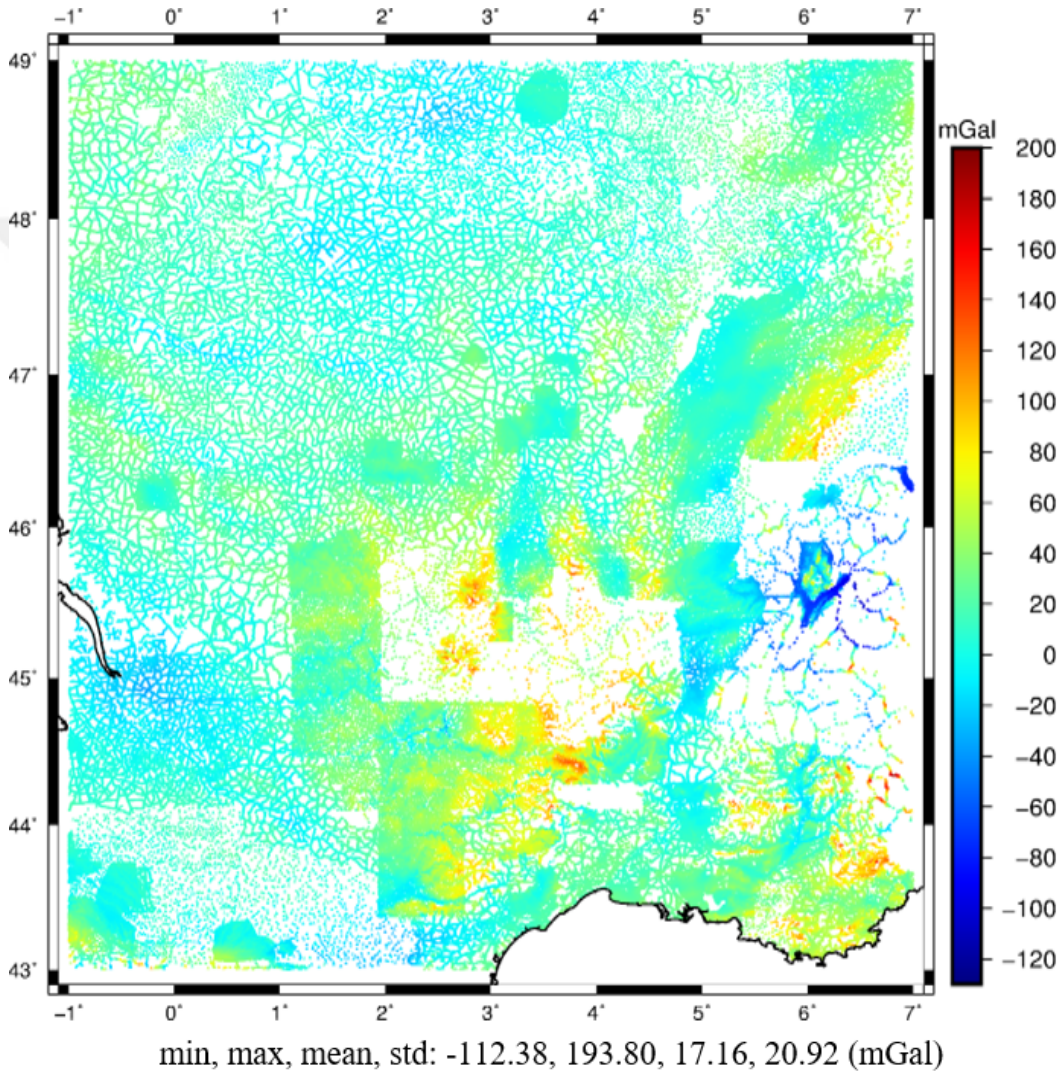


Figure 3.3 : Auvergne gravity disturbances

In order to determine a geoid model using LSMSA, surface gravity anomalies of each data point are calculated where shown in Figure 3.4 using Eq. 2.3.

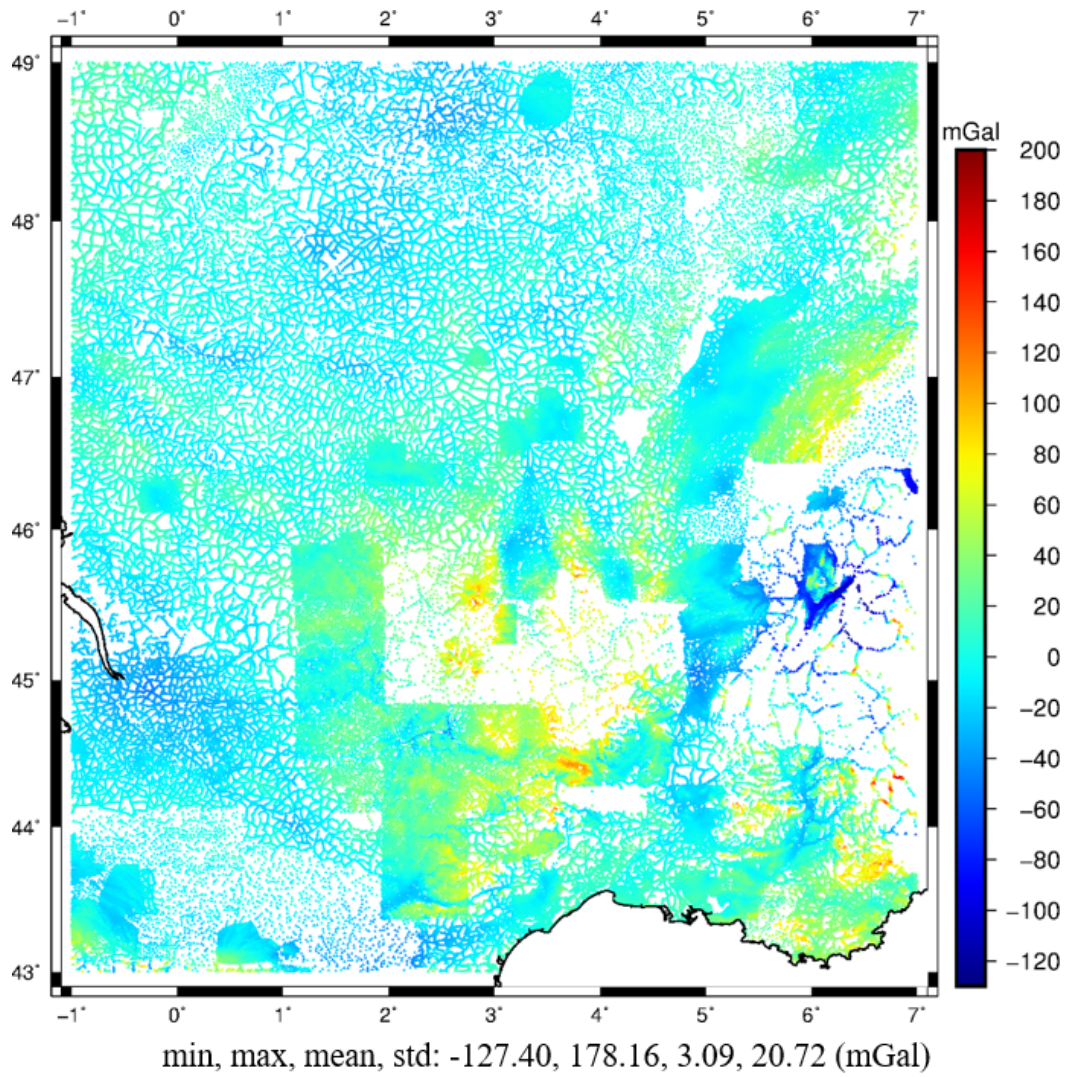
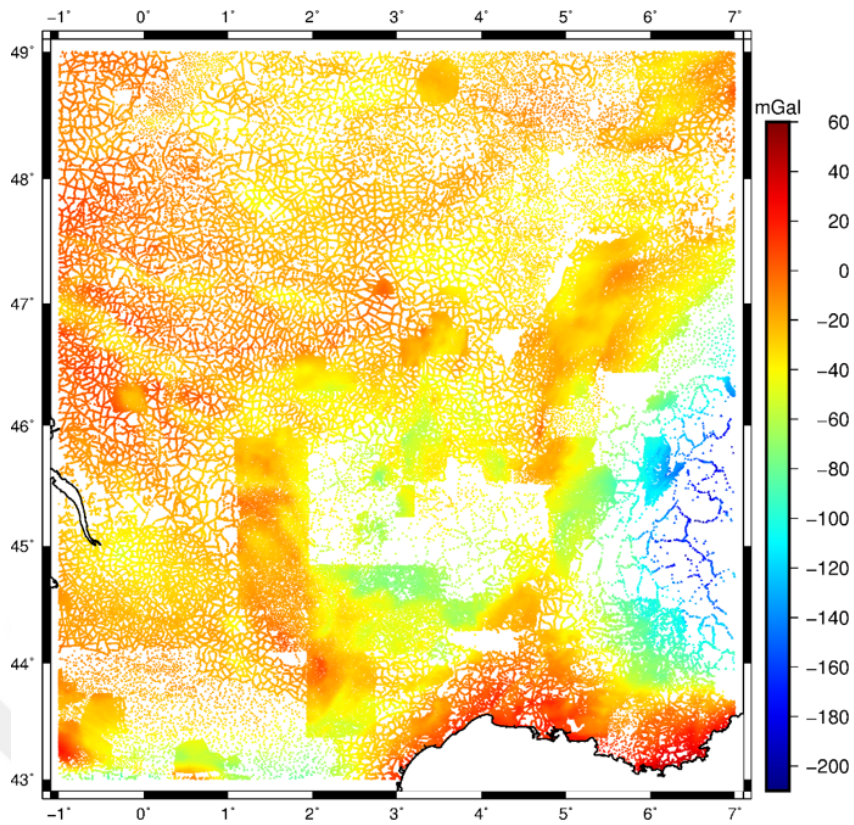


Figure 3.4 : Auvergne gravity anomalies

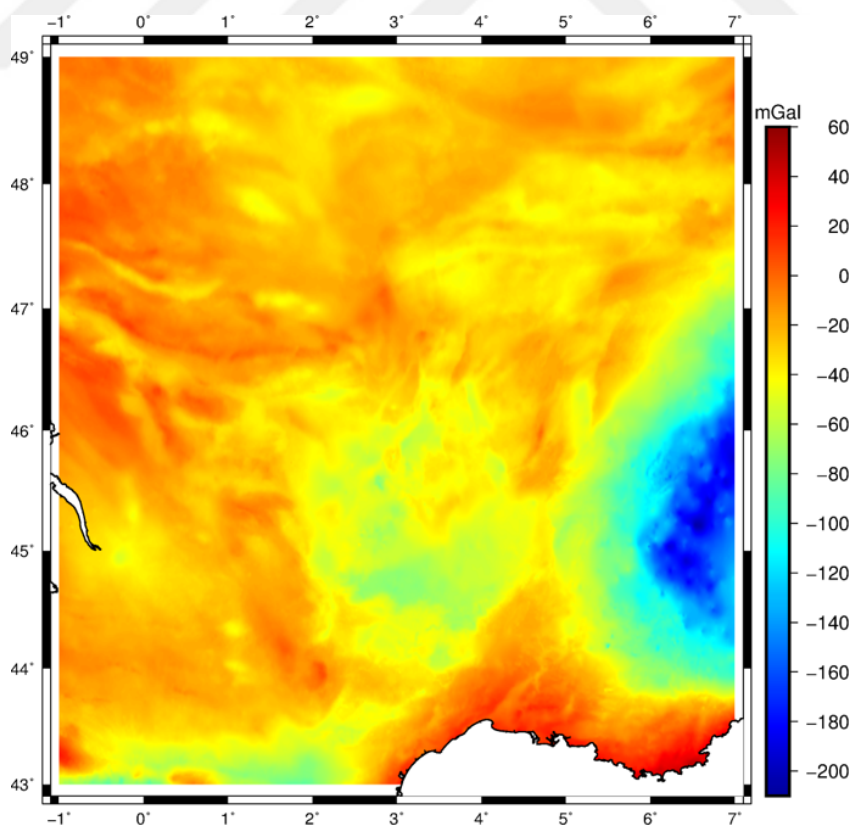
As it is mentioned in Section 2.3, it is essential that the high frequency information should be removed by reduction methods before gridding the data (Märdla et al., 2018). To do so simple Bouguer anomalies are calculated from the scattered data using Eq. 2.4. Figure 3.5 shows the simple Bouguer anomalies of data points while Figure 3.6 shows the gridded simple Bouguer anomaly values. Kriging method is used for the gridding procedure.

Once the simple Bouguer anomalies are gridded, the surface gravity anomalies are reproduced using digital elevation model given with the dataset (see Figure 3.7).



min, max, mean, std: -205.59, 56.69, -29.16, 20.81 (mGal)

Figure 3.5 : Simple Bouguer gravity anomalies



min, max, mean, std: -204.05, 57.24, -33.33, 31.68 (mGal)

Figure 3.6 : Gridded simple Bouguer gravity anomalies

In order to calculate the gravity disturbance from simple Bouguer anomaly, the geoid height needed for calculations is computed using spherical harmonic function of geoid undulation with the maximum expansion of EIGEN-6C4 (Förste et al., 2014) geopotential model. Figure 3.8 shows the gridded surface gravity disturbance values.

As it can be seen in Figure 3.7 and Figure 3.8, gravity anomaly and gravity disturbance values follow a similar trend. The reason for the change in minimum and maximum values between discrete data and the gridded data is due to the relatively high topographic change in locations where the grids are produced.

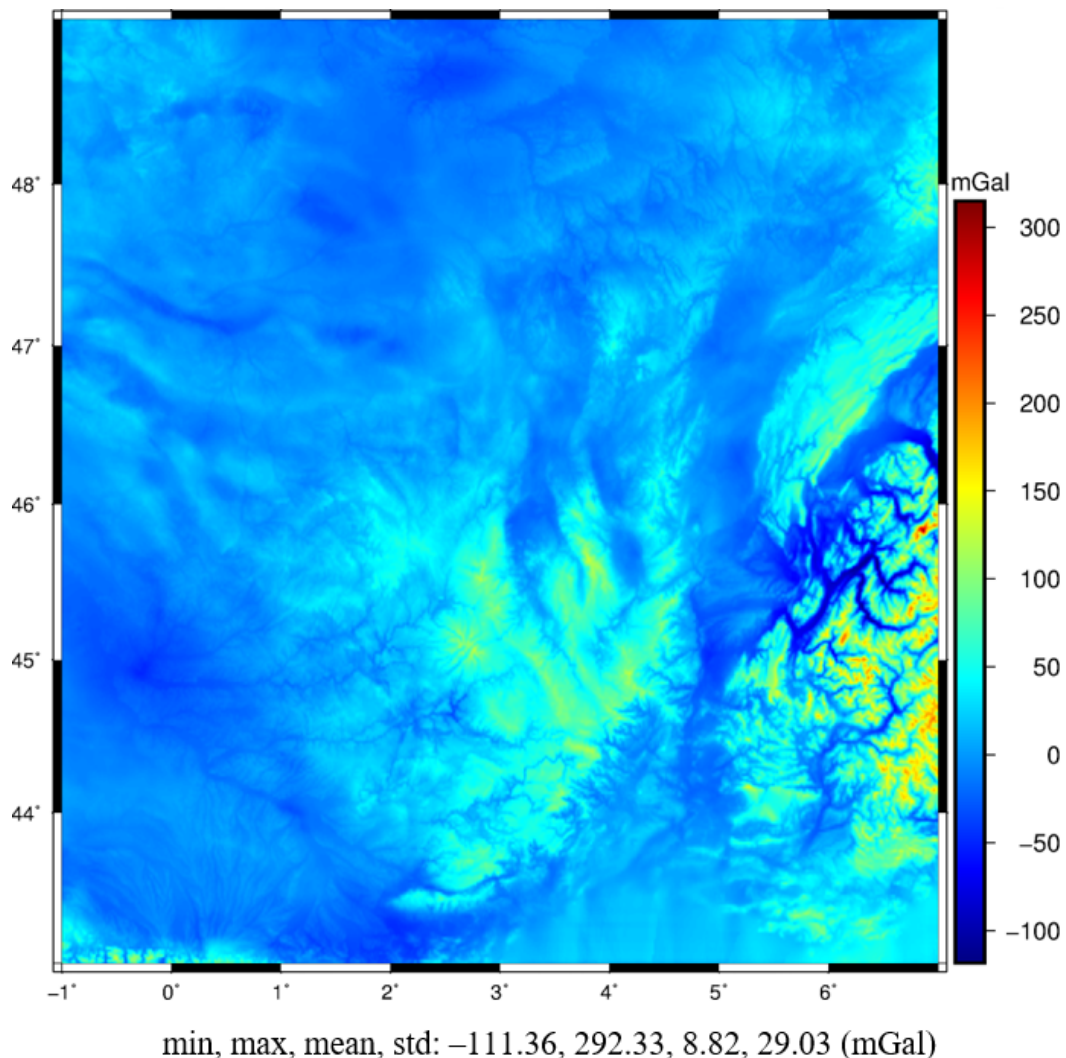
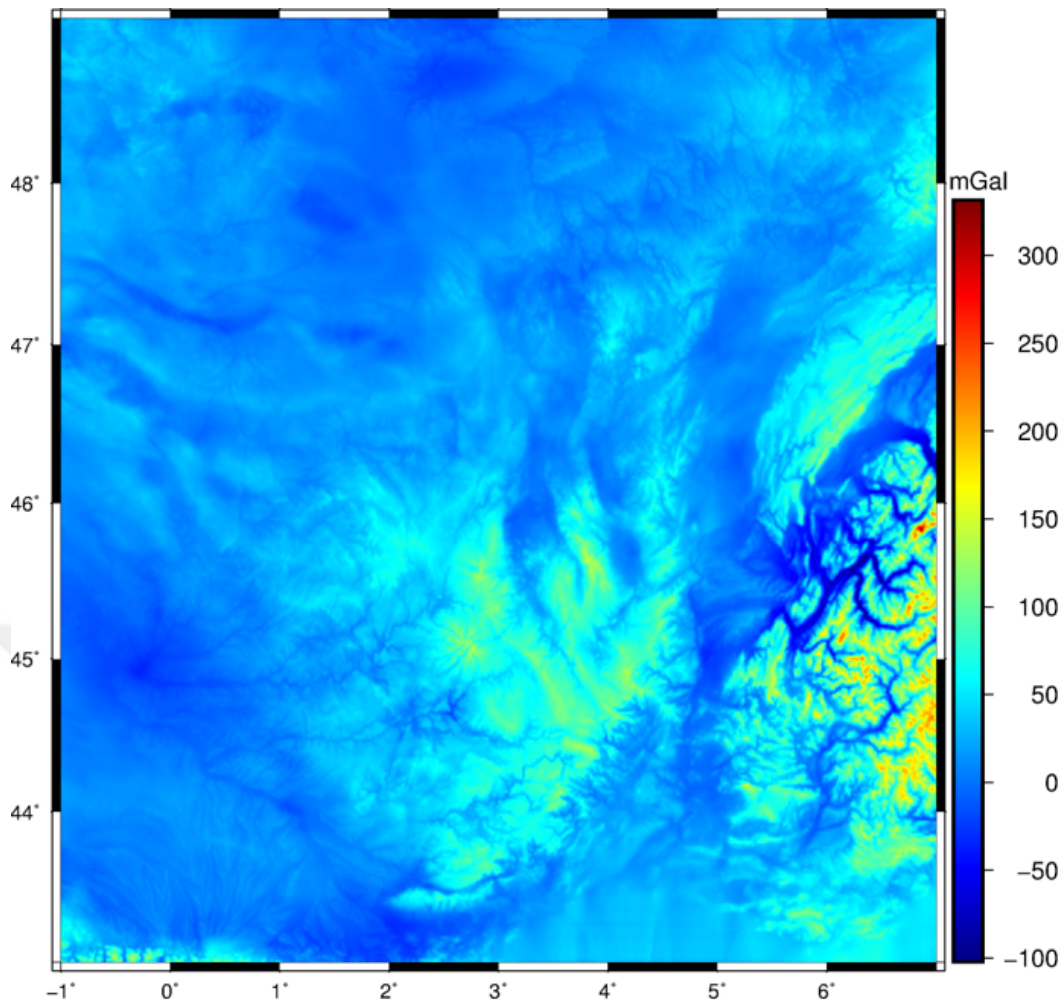


Figure 3.7 : Gridded values of Auvergne surface gravity anomalies



min, max, mean, std: -102.28, 331.60, 24.33, 29.37 (mGal)

Figure 3.8 : Gridded values of Auvergne surface gravity disturbance

3.1.2 Voronoi diagrams

In general, the gravity quantities used in the integration are the gridded values. As an alternative, discrete data is directly used in the integration partitioned with Voronoi diagrams were first introduced in Dos Santos and Escobar (2004) for geoid modeling. A Voronoi diagram is the most representative polygon surrounds the relevant computation point based on the geometrical distance between outlying points. Errors arise from gridding procedure can be eliminated using Voronoi polygons since the actual values of the gravity quantities can be directly calculated without remove-compute-restore process explained in the previous subsection. The elemental area $d\sigma$ first mentioned in Section 2.5, Eq. 2.14, corresponds to the area of each Voronoi polygon. In this study, Voronoi polygons are created using ArcGIS Pro software. Figure

3.9 shows the discrete observation points while Figure 3.10 represents the partitioned network of gravity data set using Voronoi polygons.

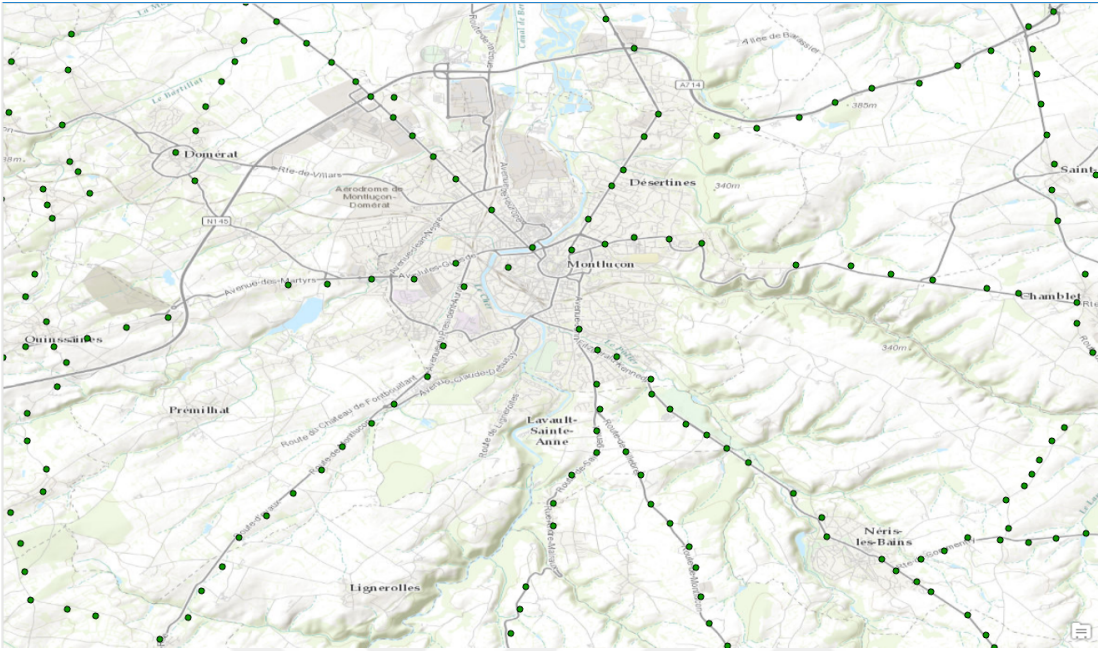


Figure 3.9 : Gravity observations in discrete form

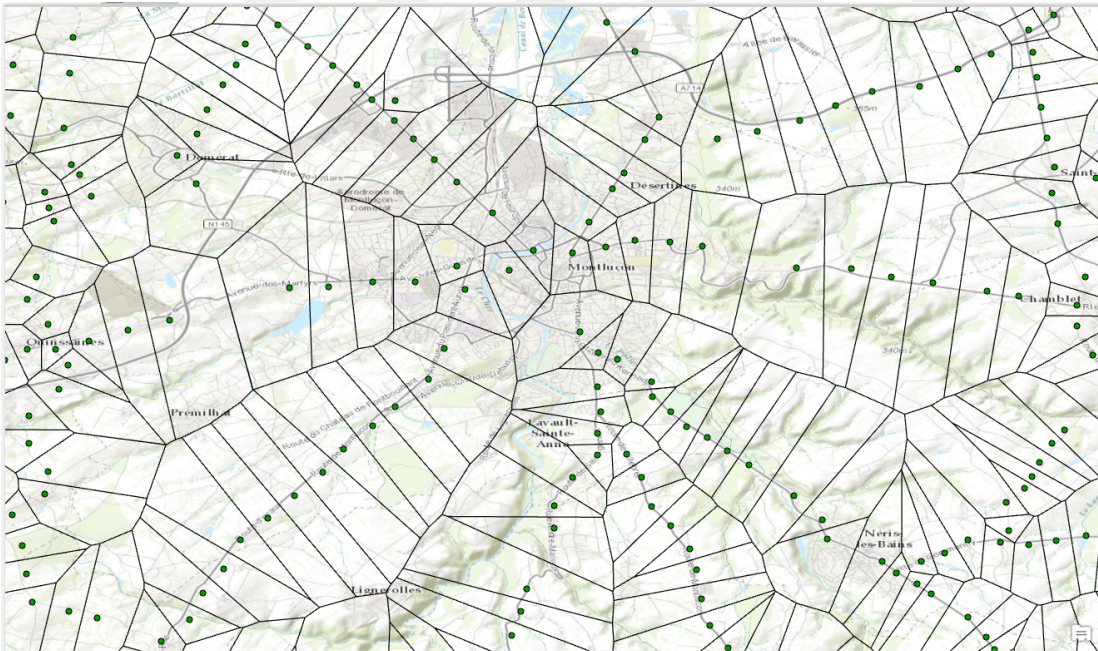


Figure 3.10 : Gravity observations partitioned according to Voronoi cell structures

It should be noted that the software or algorithm used for the creation of Voronoi polygons might result in residual areas around the boundaries of the data which cause irregularities. Hence, the polygons should be

revised manually or automatically by a proper filtering algorithm in detail to overcome such situation (see Figure 3.11, and 3.12). Additionally, data gaps might be filled beforehand using gravity quantities computed from a high resolution GGM or another data set that fits the area. In this study, gravity anomaly/disturbance grids revised manually and the integration points that produce major differences (blunders) are replaced by the values calculated from GGMs. However, no such procedure is followed for point-wise evaluation since the proper distribution and values of the actual surface gravity anomaly/disturbances cannot be determined and needs to be investigated in detail for further studies.

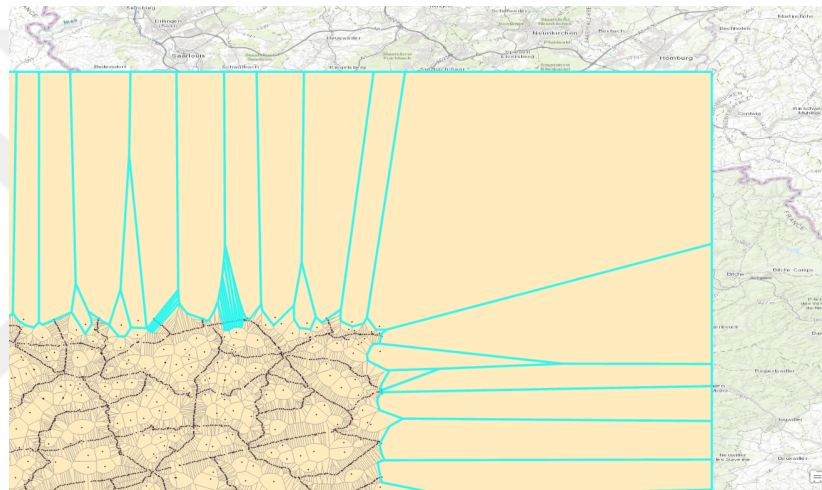


Figure 3.11 : Data borders which residual Voronoi polygons are selected

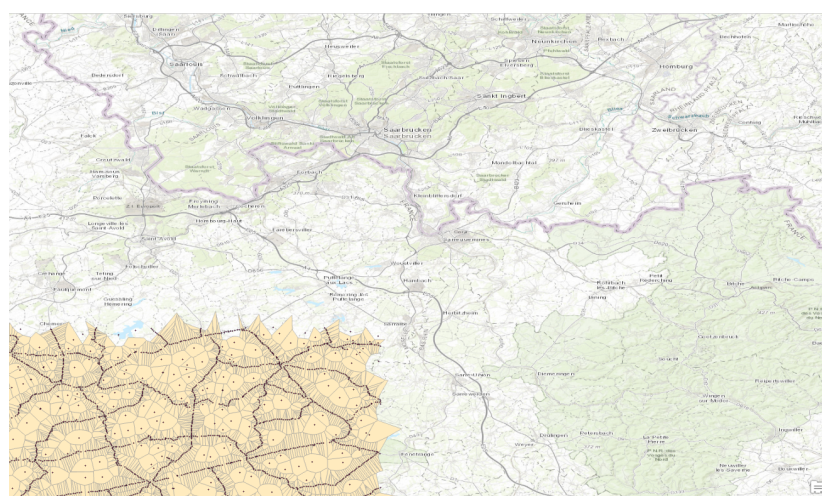


Figure 3.12 : Data borders which residual Voronoi polygons are removed

3.2 GNSS/Leveling Benchmarks

GNSS/leveling dataset includes ellipsoidal and normal heights of 75 points. The standard deviation of the ellipsoidal heights is evaluated around 2 to 3 cm as indicated in Valty et al. (2012). Distribution of GNSS/leveling benchmarks are shown as the red triangles in Figure 3.1.

Since the main emphasis of this thesis is to calculate a geoid model instead of a quasigeoid, normal height in GNSS/leveling dataset is converted to orthometric height using the relationship below:

$$\zeta - N = H - H^N \quad (3.2)$$

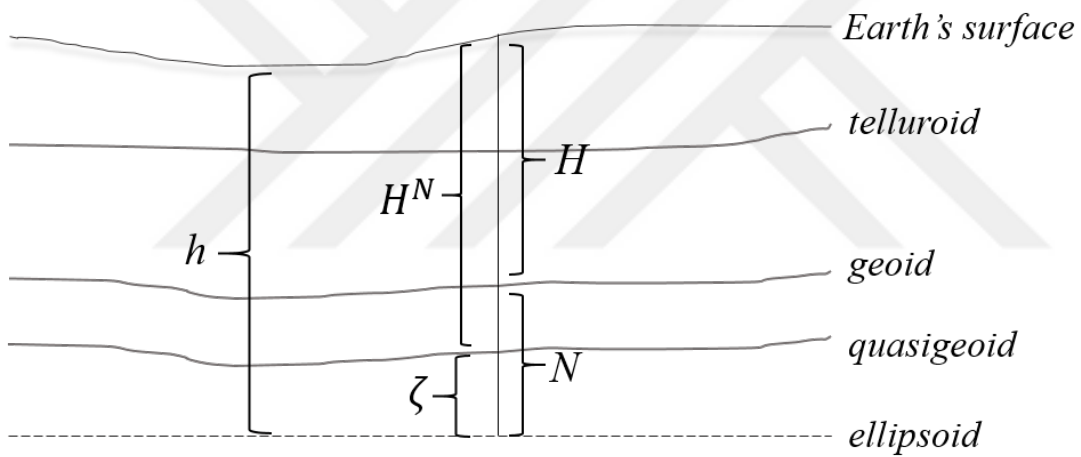


Figure 3.13 : Illustration of the height systems

where ζ , N , H^N , and H are height anomaly, geoid height, normal height, and orthometric height respectively as shown in Figure 3.13. $\zeta - N$ is calculated iteratively as (Hofmann-Wellenhof and Moritz, 2006):

$$\zeta - N \approx \frac{0.1119[m/mGal]}{9.8[m/s^2]} H^2 = 10^{-7}[m^{-1}] H^2 \quad (3.3)$$

$$\zeta - N[m] \approx 0.1 H^2[km] \quad (3.4)$$

3.3 Digital Elevation Model

The dataset provides a digital terrain model including orthometric heights for over 3 million points in grid form shown in Figure 3.14. However, since the orthometric heights of the integration points are provided by the gravity dataset, digital elevation model is not used during the calculations of combined topographic correction and combined downward continuation correction (see Section 2.6.1.1 and Section 2.6.1.2). However, it is used during the restoration of heights after gridding the simple Bouguer anomalies explained in Section 3.1.1.

Minimum, maximum, mean, and standard deviation of topographic heights in geoid computation area are 80 *m*, 1630 *m*, 460 *m*, and 270 *m* respectively.

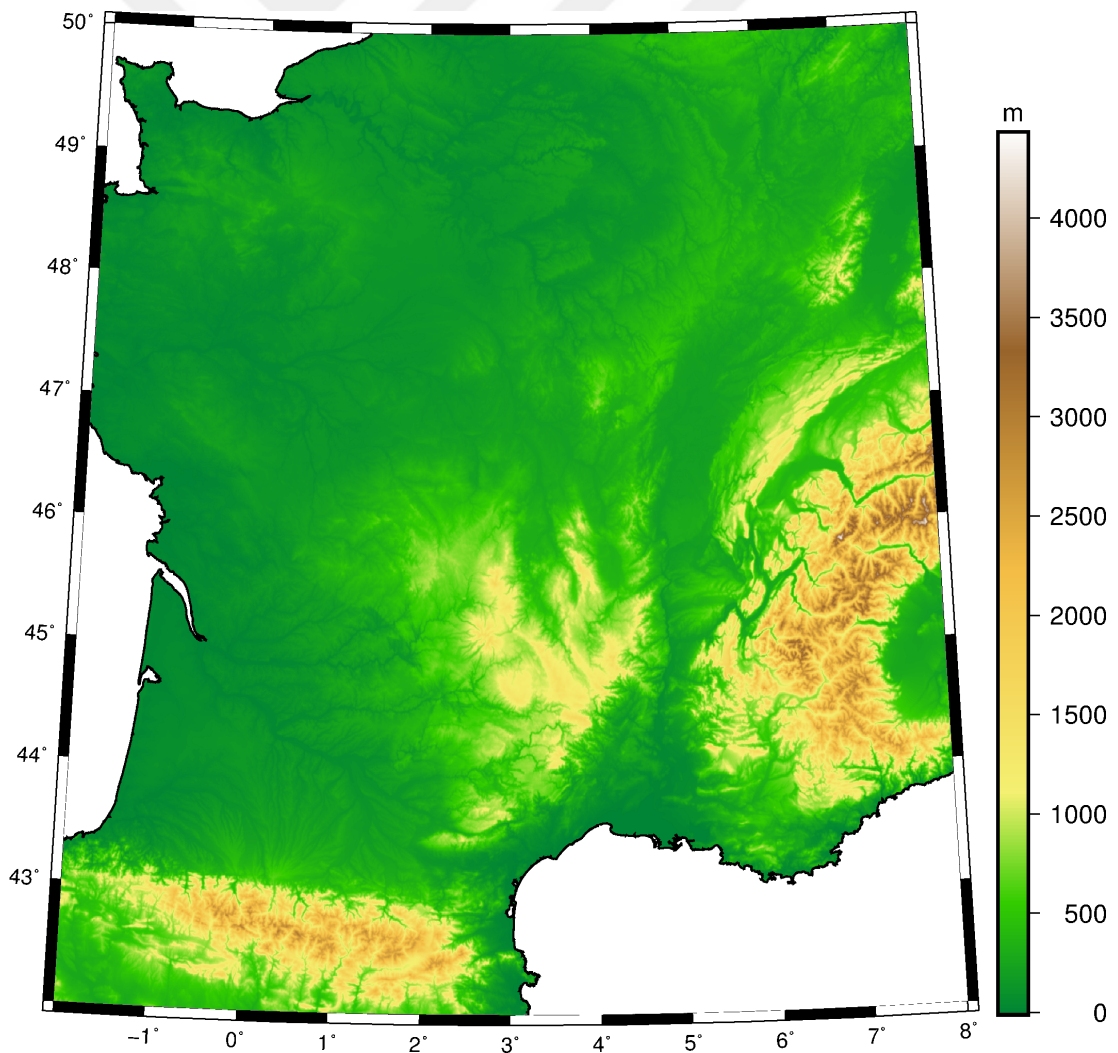


Figure 3.14 : Auvergne topography

In order to calculate the combined atmospheric correction explained in Section 2.6.1.3, it is required to compute the Laplace surface harmonics of the topographic height as (Bucha and Janák, 2017):

$$H_n(\varphi, \lambda) = \sum_{n=0}^{n_{max}} \sum_{m=0}^n \{ \overline{HC}_{nm} \cos m\lambda + \overline{HS}_{nm} \sin m\lambda \} \overline{P}_{nm}(\sin \varphi) \quad (3.5)$$

where φ and λ are latitude and longitude and \overline{HC}_{nm} and \overline{HS}_{nm} are the spherical harmonic model coefficients for Earth's elevation. In this study, Coeff_Height_and_Depth_to2190_DTM2006.0 model, available from the US National Geospatial-Intelligence Agency's (NGA) official EGM2008 website, is used up to 720 degrees.

3.4 Global Geopotential Model

Long wavelength component of geoid model is computed using spherical harmonic coefficients provided by GGMs. The performance of the final geoid model is highly dependent on the choice of the optimum geopotential model and the best degree of expansion. Thus, it is important to investigate the performance of GGMs beforehand. In this study, satellite only and combined models are tested. The list of the models are given below:

Table 3.1 : List of tested GGMs

Model	Maximum Degree of the GGM	Reference
ITG-Grace2010s	180	Mayer-Gürr et al. (2010)
GOCO05C	720	Fecher et al. (2017)

4. NUMERICAL RESULTS

4.1 Determination of Modification Parameters

In order to model an accurate geoid, the determination of the least squares modification parameters should be examined according to some sets of factors such as the GGM used, expansion degree (upper limit) of the GGM derived spherical harmonics (see M in Section 2.5), selected maximum degree of Stokes/Hotine modification (see L in Section 2.5), and the radius of the integration cap ψ_0 . In this study, M is taken equal to L and the performance of the least squares modification parameters calculated by using ITG-Grace2010 and GOCO05C global geopotential models with different expansion degrees and integration radii are investigated. Each geoid model is validated using geoid heights derived at each 75 GNSS/leveling benchmark. The standard deviation of the difference between gravimetric geoid heights and corresponding geoid heights from control data for grid-wise LSMHA procedure for biased solution is shown as "before fit" in Table 4.1. The detailed statistics of alternative geoid modeling methods which are the subjects of this study are presented in Section 4.3 according to the decisions made in this section.

As a result of the findings shown in Table 4.1 and the variance of the terrestrial data given by Valtý et al. (2012), the least squares modification parameters are calculated based on the variables shown in Table 4.2.

The computation of the least squares modification parameters are conducted by a software provided by Prof. Dr. Artu Ellmann (adopted for gravity disturbance and Hotine function for LSMHA) similar to Ellmann (2005).

Table 4.1 : Statistical results of geoid models calculated by different parameters

GGM	M=L(°)	ψ_0°	before fit (cm)
GOCO05C	120	2	6.6
GOCO05C	200	2	3.9
ITG-Grace2010	120	2	5.5
ITG-Grace2010	120	1	5.8
GOCO05C	120	1	5.1
GOCO05C	200	1	4.0
GOCO05C	200	0.5	4.7
GOCO05C	300	0.5	3.5
GOCO05C	360	0.5	3.4
GOCO05C	200	0.3	9.2
GOCO05C	300	0.3	4.6
GOCO05C	360	0.3	4.2

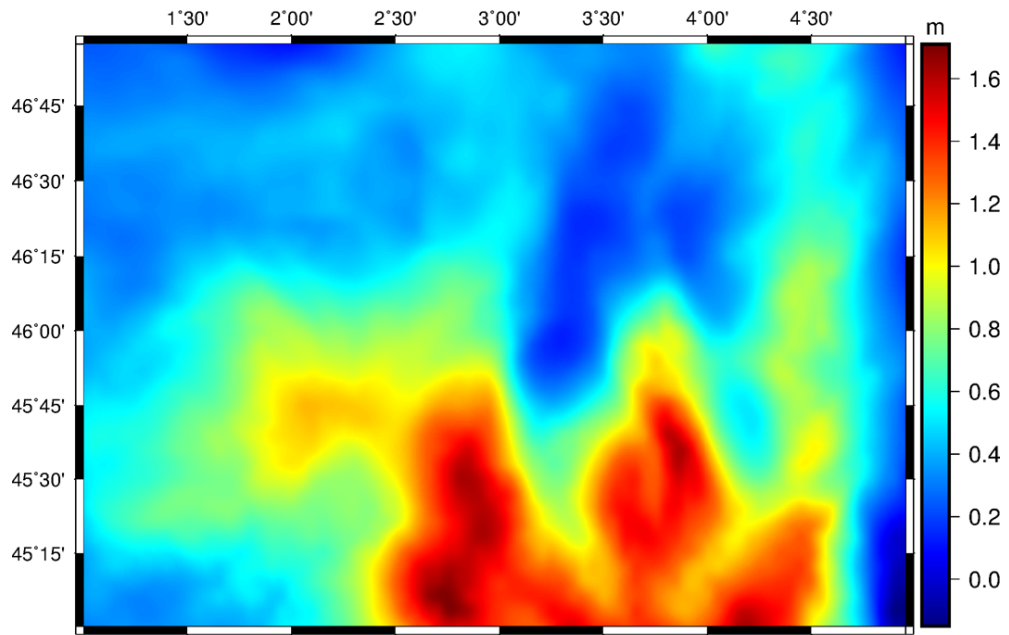
Table 4.2 : Selected parameters

Parameter	Choice
radius of the integration cap: ψ_0	0.5°
the variance of the terrestrial data: σ_n	4 $mGal^2$
Global Geopotential Model	GOCO05C
Expansion degree of the GGM: M	360°
Decomposition method	singular value decomposition

4.2 LSMHA Geoid with Components

Each component of the geoid model calculated by LSMHA evaluated by gridded gravity data are shown in this section. While the figures demonstrate the geoid model calculated using unbiased type of least squares modification parameters, the components show resemblance to the geoid models calculated by point-wise LSMHA, grid-wise LSMSA, and point-wise LSMSA.

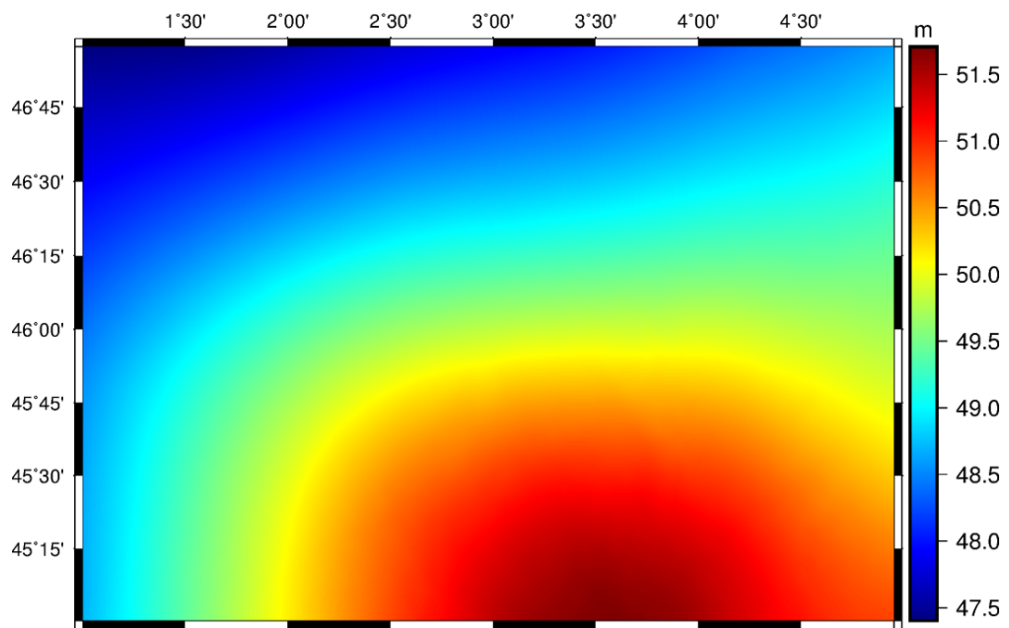
The near zone component of the geoid model calculated as the first term of Eq. 2.17 exhibits a rapidly changing surface as shown in Figure 4.1 since it represents the main deviation of geoid from leveling ellipsoid as well as the topographical effect.



min, max, mean, std: -0.1484, 1.6977, 0.6566, 0.3663 (m)

Figure 4.1 : Near zone geoid contribution computed by using grid-wise evaluation of LSMHA

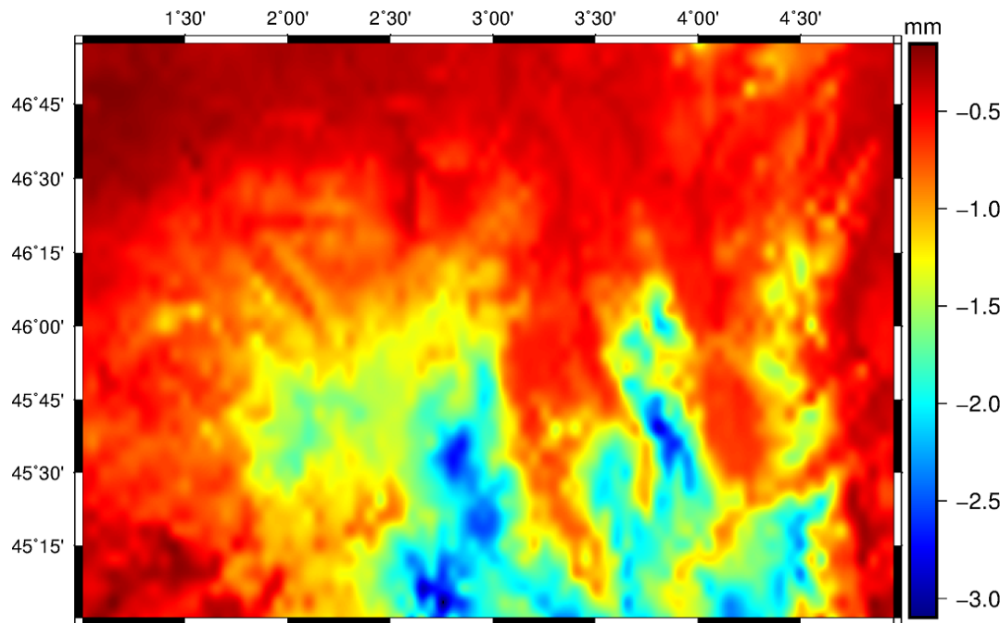
It is expected to have a smooth signal on far zone geoid since N_{far} is calculated using GGM derived spherical harmonics of gravity disturbance (second part of Eq. 2.17). As it can be seen in Figure 4.2, N_{far} constitutes the highest ratio on geoid model and represents the long wavelength component of the geoid.



min, max, mean, std: 47.4543, 52.0152, 49.6417, 1.1329 (m)

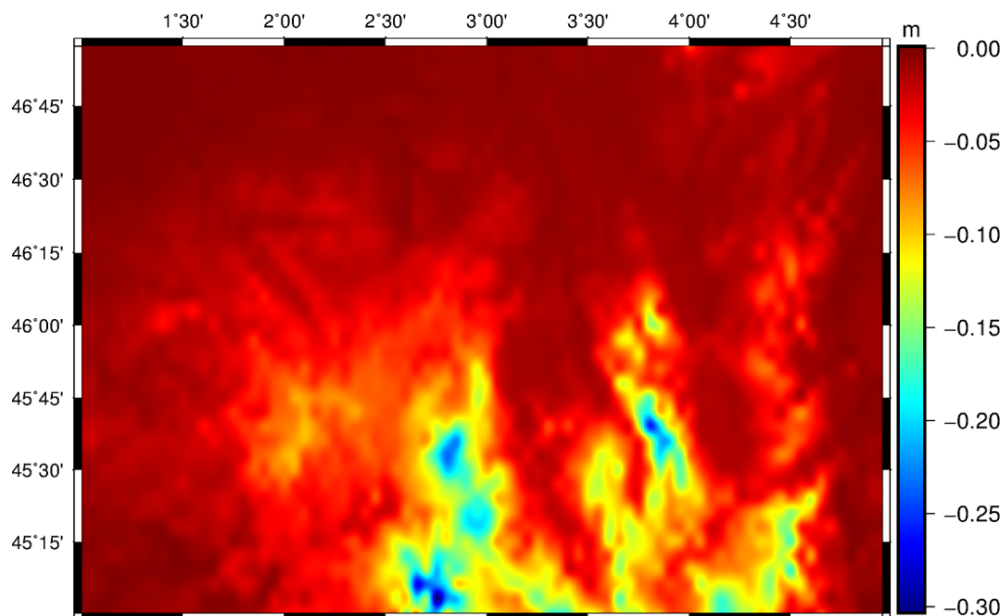
Figure 4.2 : Far zone geoid contribution computed by using grid-wise evaluation of LSMHA

Atmospheric and topographic masses cause pressure on geoid surface. The combined atmospheric correction computed using Eq. 2.29 is expected to reflect topography and shown in Figure 4.3. Additionally, the combined topographic effect is calculated using Eq. 2.23 and shown in Figure 4.4.



min, max, mean, std: -3.09, -0.15, -0.88, 0.52 (mm)

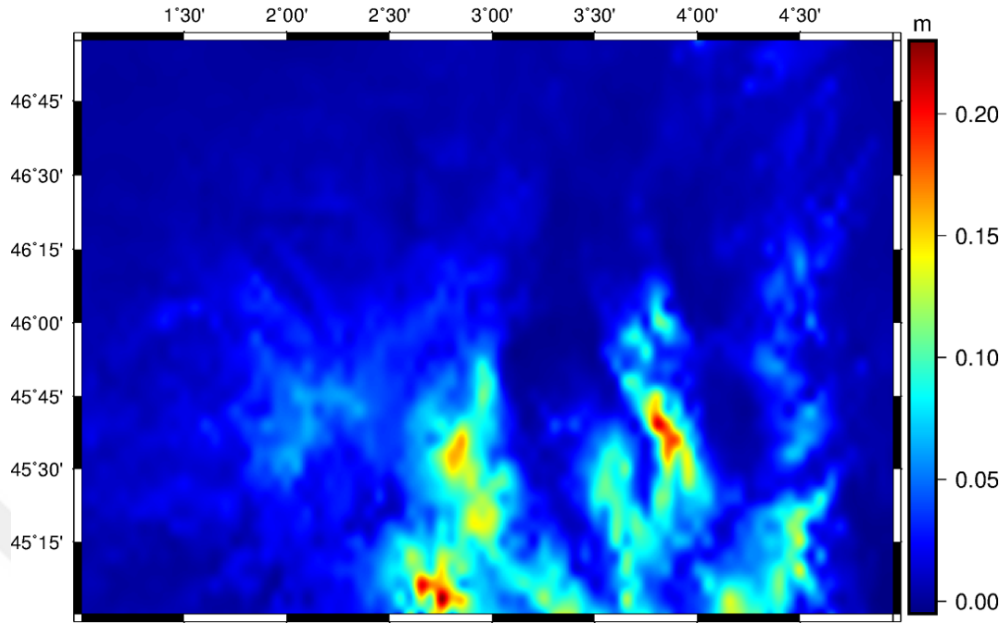
Figure 4.3 : Combined atmospheric correction on geoid model computed by using grid-wise evaluation of LSMHA



min, max, mean, std: -0.3034, -0.0007, 0.0330, 0.0392 (m)

Figure 4.4 : Combined topographic correction on geoid model computed by using grid-wise evaluation of LSMHA

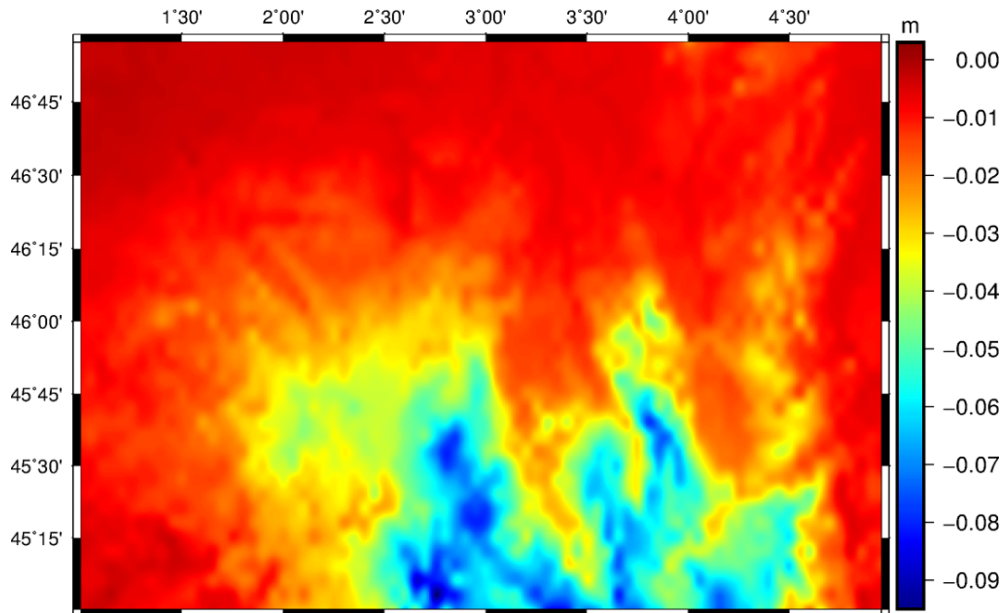
The first component of the downward continuation effect $\delta N_{DWC}^{(1)}(P)$ is calculated using Eq. 2.25 and shown in Figure 4.5.



min, max, mean, std: -0.0048, 0.2274, 0.0221, 0.0286 (m)

Figure 4.5 : $\delta N_{DWC}^{(1)}(P)$ effect on geoid model computed by using grid-wise evaluation of LSMHA

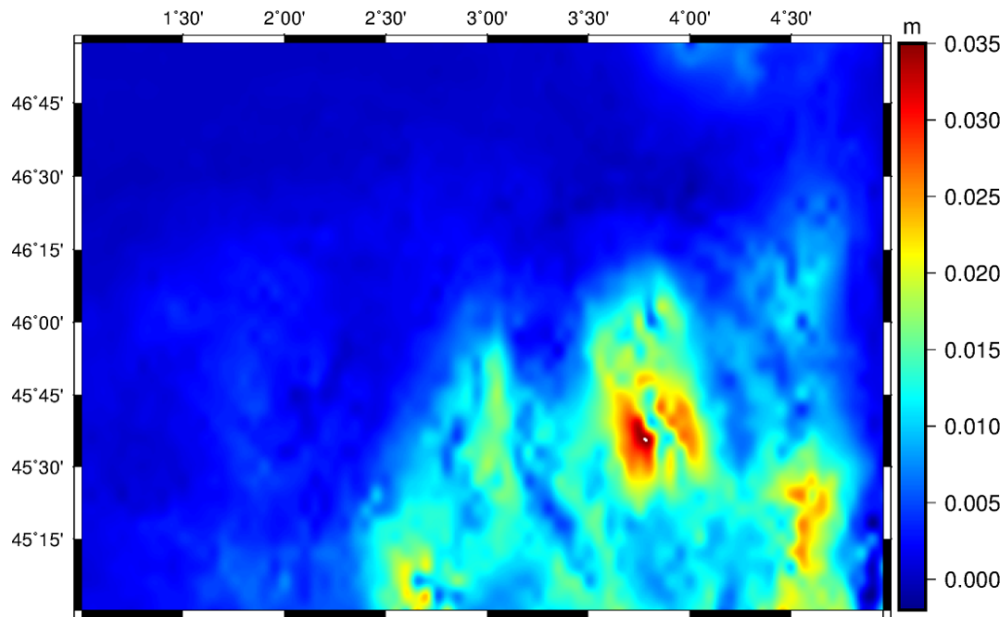
$\delta N_{DWC}^{L(1),far}(P)$ is calculated using Eq. 2.27 and shown in Figure 4.6.



min, max, mean, std: -0.0976, -0.0018, -0.0212, 0.0184 (m)

Figure 4.6 : $\delta N_{DWC}^{L(1),far}(P)$ effect on geoid model computed by using grid-wise evaluation of LSMHA

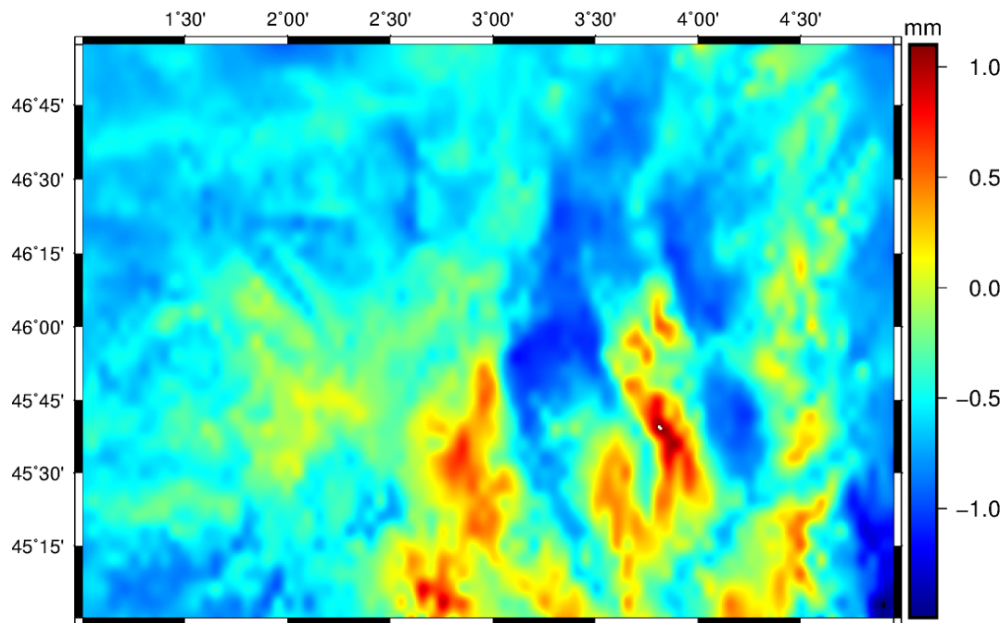
The terrain effect on combined downward continuation $\delta N_{DWC}^{L(2)}(P)$ is calculated using Eq. 2.28 and shown in Figure 4.7.



min, max, mean, std: -0.0018, 0.0343, 0.0050, 0.0055 (m)

Figure 4.7 : $\delta N_{DWC}^{L(2)}(P)$ effect on geoid model computed by using grid-wise evaluation of LSMHA

Due to the spherical approach on integration, the combined ellipsoidal correction is calculated as it represented in Eq. 2.30 and shown in Figure 4.8.



min, max, mean, std: -1.24, 0.89, -0.37, 0.27 (mm)

Figure 4.8 : Combined Ellipsoidal effect on geoid model computed by using grid-wise evaluation of LSMHA

4.3 Validation and Comparison of Resulting Geoid Models

Final geoid models are validated using GNSS/leveling derived geoid heights explained in Section 3.2. Before fit values in Table 4.3 indicate the initial statistics of the difference between gravimetric geoid model and the geoid model derived from GNSS/leveling data. In practice, corrector surface fitting procedure (Eq. 4.1) is implemented for statistical comparison in order to eliminate the factors such as systematic errors and datum inconsistencies between compared surfaces (Fotopoulos, 2003). In order to do so, 4 parameter Helmert similarity transformation is applied and the results are shown as "after fit" values in Table 4.4. BLS, ULS, and OLS stand for the solutions by biased, unbiased, and optimum types of least squares modification parameters respectively. STD and RMSE stand for the standard deviation and root mean square error.

$$\Delta N = N_{GPS} - N_{Grav} = a^T x + \epsilon \quad (4.1)$$

where a^T is the transpose of the design matrix, x is the matrix of unknowns, and ϵ represents the random noise.

4 parameters Helmert similarity transformation model is given as:

$$a_i = [1 \quad \cos \phi_i \cos \lambda_i \quad \cos \phi_i \sin \lambda_i \quad \sin \phi_i] \quad (4.2)$$

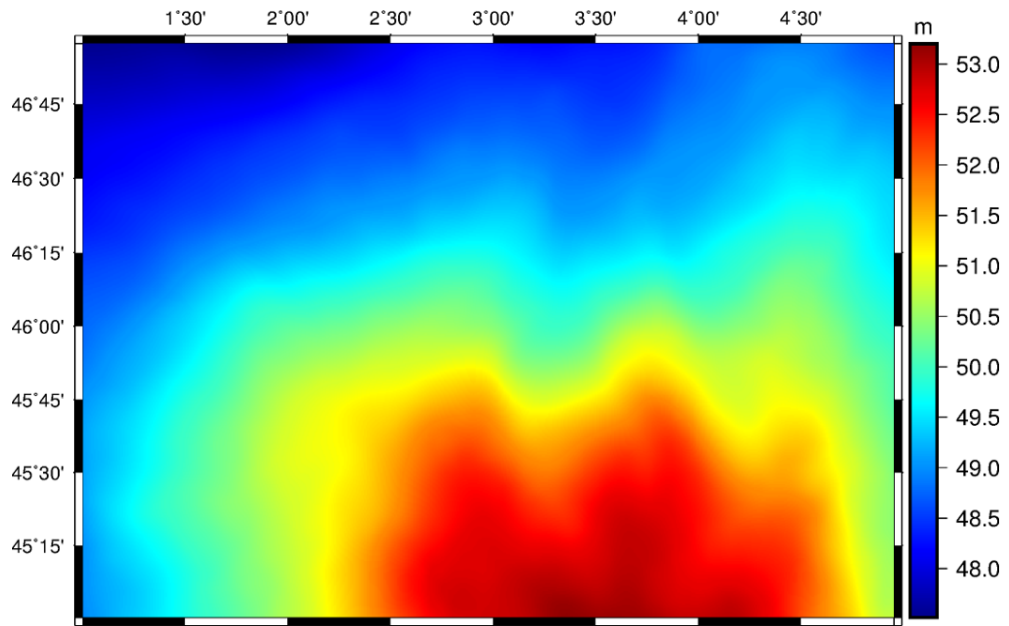
Figure 4.9, 4.10, 4.11, and 4.12 show unbiased type of geoid models computed using grid-wise and point-wise evaluation of LSMHA and LSMSA methods. However, it should be noted that the visible difference between minimum, maximum, mean, and standard deviation values stem from the systematic errors and datum inconsistencies.

Table 4.3 : Statistical results of the final geoid models: before fit (unit: m)

Method	Solution	Min	Max	Mean	STD	RMSE
LSMSA grid-wise	BLS	-1.119	-0.920	-1.025	0.045	1.026
	ULS	-1.123	-0.908	-1.025	0.046	1.026
	OLS	-1.123	-0.906	-1.025	0.046	1.026
LSMHA grid-wise	BLS	-0.961	-0.791	-0.890	0.034	0.890
	ULS	-0.963	-0.783	-0.890	0.035	0.890
	OLS	-0.963	-0.779	-0.890	0.035	0.890
LSMSA point-wise	BLS	-1.088	-0.818	-0.988	0.062	0.990
	ULS	-1.093	-0.818	-0.993	0.061	0.995
	OLS	-1.094	-0.818	-0.995	0.060	0.997
LSMHA point-wise	BLS	-0.935	-0.705	-0.848	0.053	0.849
	ULS	-0.940	-0.705	-0.854	0.052	0.856
	OLS	-0.942	-0.705	-0.856	0.052	0.858

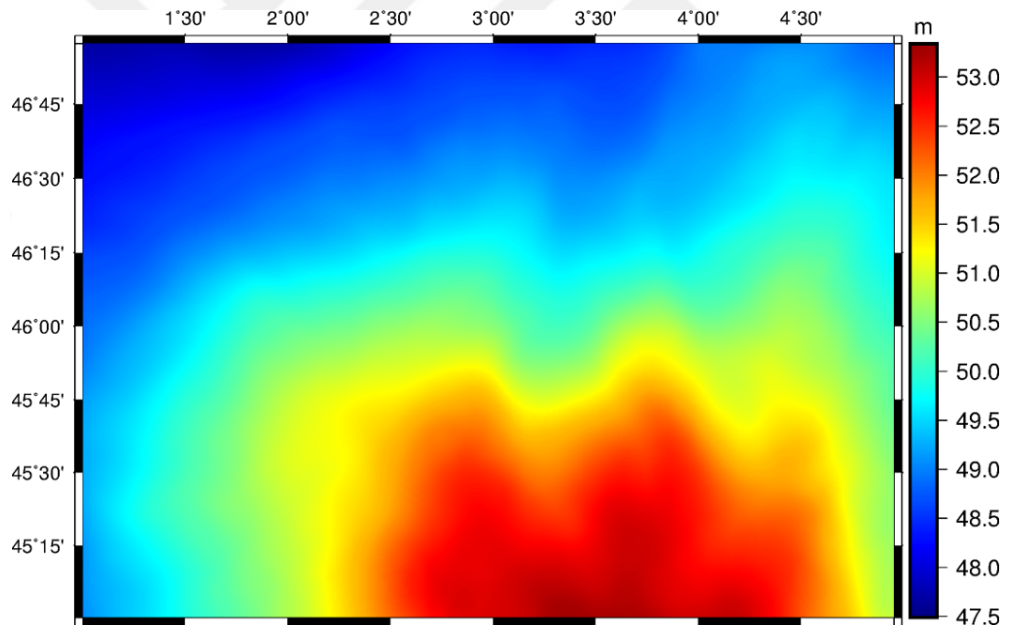
Table 4.4 : Statistical results of the final geoid models: after fit (unit: m)

Method	Solution	Min	Max	Mean	STD	RMSE
LSMSA grid-wise	BLS	-0.056	0.105	0.000	0.028	0.028
	ULS	-0.056	0.114	0.000	0.028	0.028
	OLS	-0.057	0.117	0.000	0.029	0.029
LSMHA grid-wise	BLS	-0.062	0.106	0.000	0.028	0.028
	ULS	-0.063	0.115	0.000	0.028	0.028
	OLS	-0.063	0.118	0.000	0.029	0.029
LSMSA point-wise	BLS	-0.107	0.104	0.000	0.043	0.043
	ULS	-0.104	0.112	0.000	0.043	0.043
	OLS	-0.104	0.114	0.000	0.044	0.044
LSMHA point-wise	BLS	-0.116	0.107	0.000	0.043	0.043
	ULS	-0.112	0.117	0.000	0.045	0.045
	OLS	-0.110	0.120	0.000	0.045	0.045



min, max, mean, std: 47.5164, 53.2017, 50.1123, 1.4123 (m)

Figure 4.9 : Final geoid from grid-wise evaluation of LSMHA



min, max, mean, std: 47.6622, 53.3054, 50.2499, 1.4026 (m)

Figure 4.10 : Final geoid from grid-wise evaluation of LSMSA

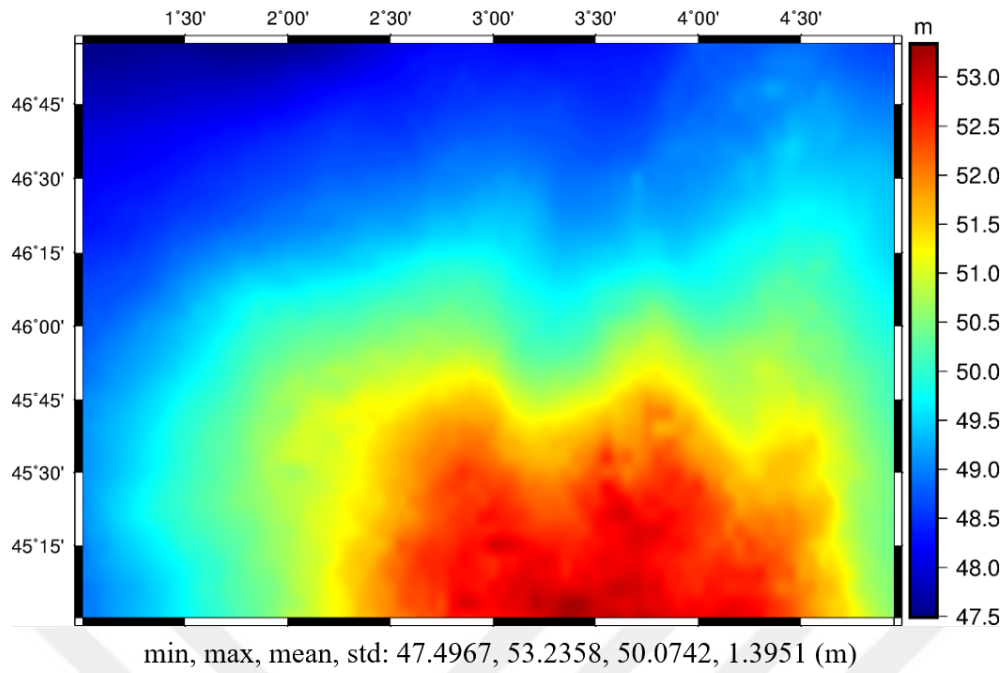


Figure 4.11 : Final geoid from point-wise evaluation of LSMHA

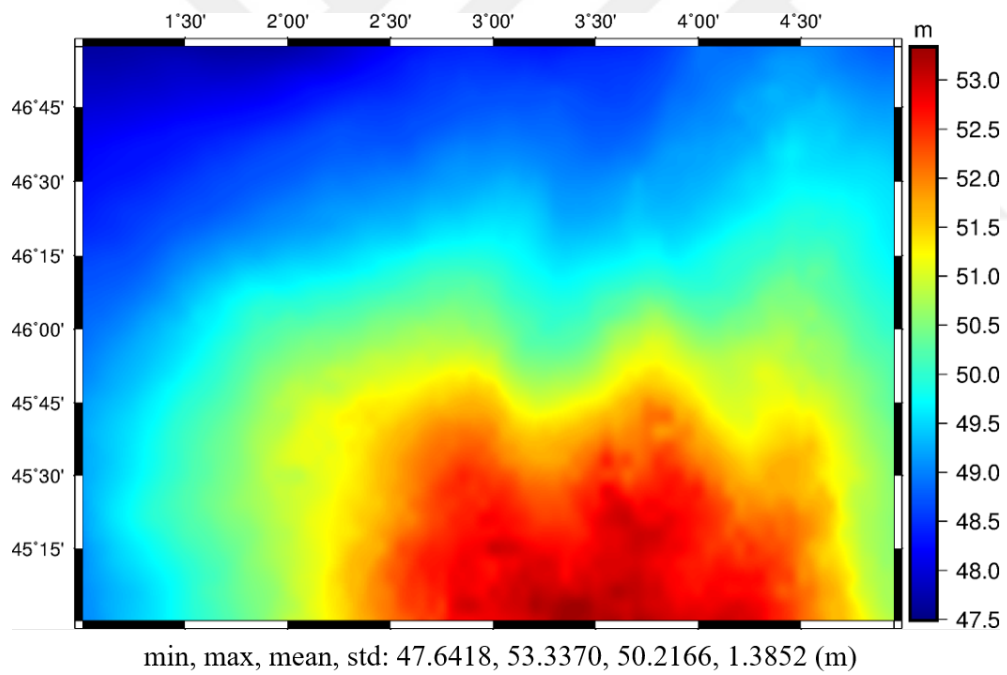


Figure 4.12 : Final geoid from point-wise evaluation of LSMSA

5. COMPUTATIONAL DIFFICULTIES

It is well known, a considerable amount of changes on the scripts/software are applied to achieve the optimum high resolution geoid model. In order to enhance the running speed of the scripts, several approaches are followed:

- Increasing the grid size of the geoid model to be computed
- Profiling
- Pre-alignment
- Vectorization
- Limiting the integration area
- 3D matrix solutions
- Parallel processing

In this study, local geoid models with 1 minute resolution are calculated. However, during the tests, the spacing is increased to 3 minutes to obtain quicker results. Apart from this, an initial geoid model can be computed for tests only in the locations of the GNSS/leveling network to enhance the speed. This approach can also be considered as a more factual treatment since the errors caused by interpolation from geoid model to the GNSS/leveling points are eliminated for the validation procedure at the first place.

Secondly, profiling technique can be used which is not a tool that improves the performance of the code; but, enables to determine the time-consuming section of the functions. In addition to that, it is necessary to determine the size of a variable beforehand which is called pre-alignment. While optimizing the algorithm, it is advised to use vector arrays and vector operations to increase the performance.

Calculation of the Stokes/Hotine function requires spherical distances between computation point and the running points located within the integration cap. While conducting an integration using gridded data, one can calculate the spherical distances and use the same values by shifting the integration area. However, point-wise evaluation requires variant spherical distances for each running point. To reduce the running time, a preliminary limitation on integration area should be implemented. Red square represents the initial limit where shown in Figure 5.1.

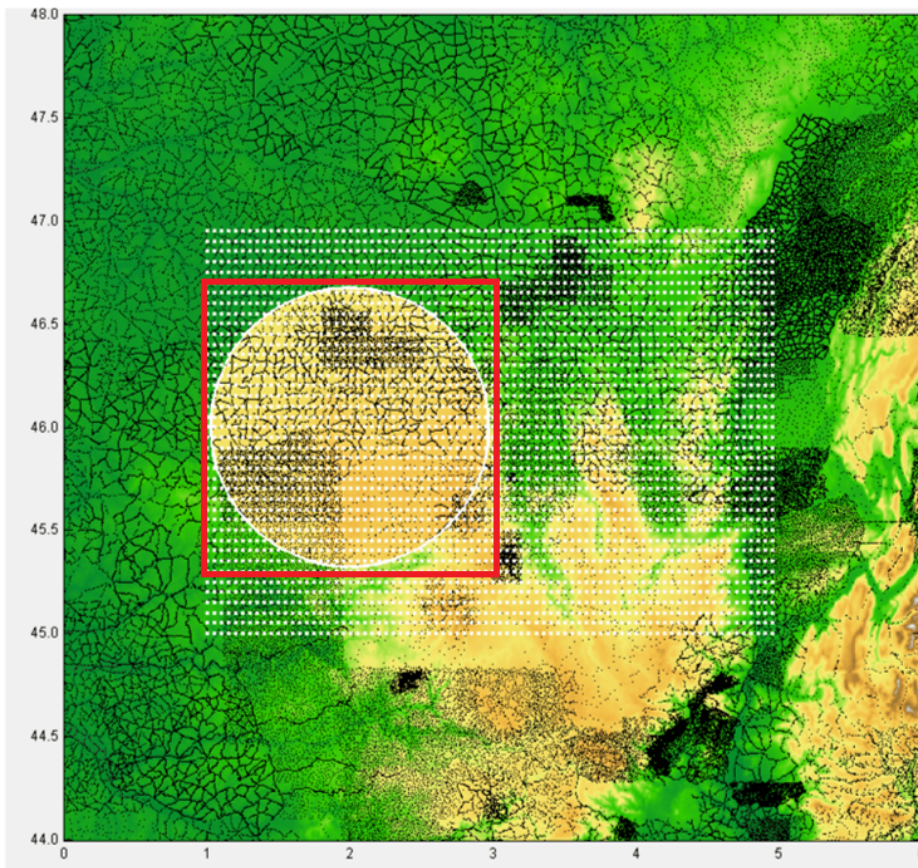


Figure 5.1 : Limitation on the integration area

Some procedures require series expansions of variables such as gravity disturbance/anomaly in far zone contribution of geoid or harmonic heights used in atmospheric correction (see Eq. 2.19 and Eq. 3.5). Hence the computation of those variables each time of operation is time-consuming, those variables can be stored in 3 dimensional matrices and imported as an input for the following executions. Matrices can be designed to store

latitude, longitude, and the related variable up to preferred degree for each computation point as shown in Figure 5.2.

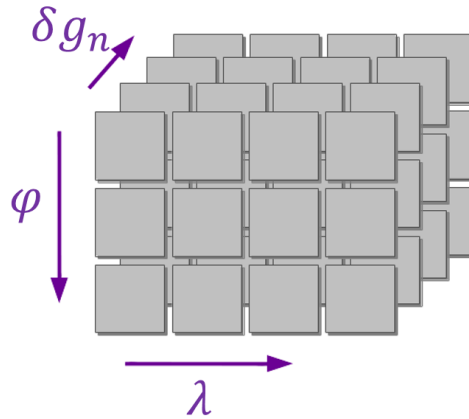


Figure 5.2 : 3D matrix

Apart from all the techniques mentioned above, the algorithm used in this study is modified to be suitable for parallel processing. By doing so, the running time of the whole geoid modeling procedure is improved 3.7 times faster when connecting 4 workers (speed is dependent on the number of connected workers). It is critical to send independent processes to each worker instead of conducting an iterative solution. As a prior check, it is strongly advised to control the results from regular code and parallel code since an unnecessary connection may cause irregularities in results. Finally, the execution time for point-wise evaluation of 1 minute resolution geoid model in Auvergne area where the total number of computation points is 28800; is recorded as 2h30'. The hardware used in the computations has 4-cored i7 processor with the base speed of 2.40 GHz.



6. CONCLUSIONS

In this study, regional geoid modeling methods are investigated in sense of grid-wise and point-wise evaluation. The geoid models in Auvergne area are created using grid-wise LSMSA, grid-wise LSMHA, point-wise LSMSA, and point-wise LSMHA methods. In order to validate the models, GNSS/leveling derived geoid heights including 75 points representing the area provided by the dataset are used as control points. The standard deviation of the differences from control network to gravimetric geoid models are calculated (before fit). Consequently, LSMHA method showed superior results to LSMSA approach for both grid-wise and point-wise approaches. For grid-wise evaluation LSMHA and LSMSA methods displayed performance of 3.4 cm and 4.5 cm accuracy respectively for biased solution (almost identical for unbiased and optimum type of solutions). As for the point-wise integration, the standard deviation of the error of geoid model calculated using LSMSA is 6.2 cm where the corresponding value is 5.3 cm for LSMHA counterpart (see Table 4.3). For that matter, it is deduced that the Hotine approach is more reliable than Stokes in an area where the change in topographic heights is noticeable. However, after corrector surface fitting using 4 parameters Helmert similarity transformation is performed, it is revealed that the final accuracy of those two methods is indicated almost identical results as shown in Table 4.4. The difference on the accuracies between the initial statistical evaluation (before fit) and after corrector surface fitting (after fit) is considered as due to the systematic errors and datum inconsistencies.

After the gridding procedure, the minimum and the maximum values of gravity quantities change noticeably (see Section 3.1.1). This might be due to the absence of gravity observations in the grid locations where produced synthetically using digital elevation model. On the contrary, the original signal of gravity data is preserved during point-wise integration since the calculation

of the gravity quantities is directly performed at the observed location. In addition to that, it is known that the gridding method can also be considered as a source of error by nature. In this context, this study aimed to perform a more accurate geoid modeling method using point-wise integration. However, statistics showed that, grid-wise evaluation of both LSMSA and LSMHA methods are considered more accurate compared to point-wise approach. After fit statistics showed that the point-wise geoid is 4.3 cm accurate while the grid-wise is 2.8 cm (Table 4.4).

In order to determine the inadequacy of point-wise integration, the issue should be investigated in sense of the gravity data and the method used. As for the data, it is associated with a prior filtering on discretely distributed gravity data or filling the data gaps with gravity quantities matching the area might be needed before the integration. In regard to the method used, primarily the elimination method of singularity must be investigated in detail where the method introduced in this thesis constitutes the novelty of this study. Singularity problem causes from the integration of gravity data which is located at the computation point or nearby. For the grid-wise evaluation, singularity elimination methods are employed which are conducted in previous studies as explained in Section 2.7.1. Analogously, as an alternative implementation for point-wise evaluation; the integration point which is the closest to the computation point is taken into account as the source of singularity in this study. Apart from the singularity problem, in order to improve the point-wise approach; it is advised to examine the calculation method of the particular area for each surface element $d\sigma$ (see Eq. 2.14) since a rough approximation is followed during the computations in this thesis.

In order to test a gravimetric geoid model, a need for higher accuracy on validation data is still needed to conduct a more realistic comparison. Additionally, the accuracy and the density of the gravity observations are highly related to the final accuracy of the model which should be improved.

The major computational obstacle and time-consuming part confronted in this study can be represented as the calculation of the modified Stokes/Hotine kernel. In order to compute the modified Stokes/Hotine function, the

spherical distances between the computation point and the integration points are calculated and un-normalized Legendre polynomials are computed for each. Using gravity grids may overcome the time-consuming part of this procedure since the spherical distance of the computation and integration points will remain the same for sequent grids. However, discrete evaluation requires calculation of integration distances separately for each data point since there is no a uniform distribution exist. To improve the efficiency and the computation time of the algorithm, the codes are modified to be suitable for parallel processing. For future studies, it is also advised to modify the algorithm using object-oriented structure where such optimization on coding experience can result in a better performance.





REFERENCES

- Abbak, R. A. and Ustun, A.** (2015). A software package for computing a regional gravimetric geoid model by the KTH method. *Earth Science Informatics*, 8(1):255–265.
- Ågren, J.** (2004). *Regional geoid determination methods for the era of satellite gravimetry: numerical investigations using synthetic earth gravity models*. PhD thesis, Infrastruktur.
- Ågren, J. and Sjöberg, L. E.** (2014). Investigation of gravity data requirements for a 5 mm quasigeoid model over Sweden. In *Gravity, Geoid and Height Systems*, pages 143–150. Springer.
- Ågren, J., Sjöberg, L. E., and Kiamehr, R.** (2009). The new gravimetric quasigeoid model KTH08 over Sweden. *Journal of Applied Geodesy*, 3(3):143–153.
- Barthelmes, F.** (2009). Definition of functionals of the geopotential and their calculation from spherical harmonic models. [http://publications.iass-potsdam.de/pubman/item/escidoc,104132\(3\):0902-2](http://publications.iass-potsdam.de/pubman/item/escidoc,104132(3):0902-2).
- Bayoud, F. A. and Sideris, M. G.** (2003). Two different methodologies for geoid determination from ground and airborne gravity data. *Geophysical Journal International*, 155(3):914–922.
- Bruns, H.** (1878). *Die figur der erde*. Berlin, P. Stankiewicz, 1878.
- Bucha, B. and Janák, J.** (2017). Definition of functionals of the geopotential used in Graflab software.
- Dos Santos, N. and Escobar, I.** (2004). Discrete evaluation of Stokes's integral by means of Voronoi and Delaunay structures. *Journal of Geodesy*, 78(6):354–367.
- Ellmann, A.** (2001). *Least squares modification of Stokes formula with application to the Estonian geoid*. Institutionen för geodesi och fotogrammetri,.
- Ellmann, A.** (2004). *The geoid for the Baltic countries determined by the least squares modification of Stokes formula*. PhD thesis, Infrastruktur.
- Ellmann, A.** (2005). Computation of three stochastic modifications of Stokes's formula for regional geoid determination. *Computers & Geosciences*, 31(6):742–755.

- Farahani, H. H., Klees, R., and Slobbe, C.** (2017). Data requirements for a 5 mm quasigeoid in the Netherlands. *Studia Geophysica et Geodaetica*, 61(4):675–702.
- Fecher, T., Pail, R., Gruber, T., Consortium, G., et al.** (2017). GOCO05C: A new combined gravity field model based on full normal equations and regionally varying weighting. *Surveys in Geophysics*, 38(3):571–590.
- Förste, C., Bruinsma, S., Abrikosov, O., Flechtner, F., Marty, J.-C., Lemoine, J.-M., Dahle, C., Neumayer, H., Barthelmes, F., König, R., et al.** (2014). EIGEN-6C4 the latest combined global gravity field model including GOCE data up to degree and order 1949 of GFZ Potsdam and GRGS Toulouse. In *EGU General Assembly Conference Abstracts*, volume 16.
- Fotopoulos, G.** (2003). *An analysis on the optimal combination of geoid, orthometric and ellipsoidal height data*. University of Calgary, Department of Geomatics Engineering.
- Freedon, W., Nashed, M., and Sonar, T.** (2015). *Handbook of Geomathematics: Second Edition*.
- Heiskanen, W. A. and Moritz, H.** (1967). Physical geodesy. *Bulletin Géodésique (1946-1975)*, 86(1):491–492.
- Hofmann-Wellenhof, B. and Moritz, H.** (2006). *Physical geodesy*. Springer Science & Business Media.
- Hotine, M.** (1969). *Mathematical Geodesy*. Washington, US Environmental Science Services Administration; [for sale by the Supt. of Docs., US Govt. Print. Off.] 1969.
- Işık, M. S.** (2016). *An Investigation On The Contribution Of GOCE Satellite Mission To Regional Geoid Modelling in Turkey*. MSc thesis, Istanbul Technical University, Graduate School of Science, Engineering and Technology.
- Janák, J., Vaňiček, P., Foroughi, I., Kingdon, R., Sheng, M. B., and Santos, M. C.** (2017). Computation of precise geoid model of Auvergne using current UNB Stokes-Helmert's approach. *Contributions to Geophysics and Geodesy*, 47(3):201–229.
- Jekeli, C.** (1979). Global accuracy estimates of point and mean undulation differences obtained from gravity disturbances, gravity anomalies and potential coefficients. Report 288. The Ohio State University.
- Kiamehr, R.** (2006). *Precise Gravimetric Geoid Model for Iran Based on GRACE and SRTM Data and the Least-Squares Modification of Stokes' Formula: with Some Geodynamic Interpretations*. PhD thesis, KTH.
- Li, Y.** (2000). *Airborne gravimetry for geoid determination*. PhD thesis.

- Listing, J.** (1873). Ueber unsere jetzige kenntniss der gestalt und groesse der erde.
- Märdla, S., Ågren, J., Strykowski, G., Oja, T., Ellmann, A., Forsberg, R., Bilker-Koivula, M., Omang, O., Paršeliūnas, E., Liepinš, I., et al.** (2017). From discrete gravity survey data to a high-resolution gravity field representation in the Nordic-Baltic region. *Marine Geodesy*, 40(6):416–453.
- Märdla, S., Ellmann, A., Ågren, J., and Sjöberg, L. E.** (2018). Regional geoid computation by least squares modified Hotine's formula with additive corrections. *Journal of Geodesy*, 92(3):253–270.
- Mayer-Gürr, T., Eicker, A., Kurtenbach, E., and Ilk, K.-H.** (2010). ITG-GRACE: global static and temporal gravity field models from GRACE data. In *System Earth via geodetic-geophysical space techniques*, pages 159–168. Springer.
- Molodensky, M.** (1962). Methods for study of the external gravitational field and figure of the Earth. *Jerusalem, Israel Program for Scientific Translations, 1962*; [available from the Office of Technical Services, US Dept. of Commerce, Washington].
- Paul, M.** (1973). A method of evaluating the truncation error coefficients for geoidal height. *Bulletin Géodésique (1946-1975)*, 110(1):413–425.
- Sjöberg, L. E. and Bagherbandi, M.** (2017). *Gravity Inversion and Integration*. Springer.
- Sjöberg, L. E.** (1984). *Least squares modification of Stokes' and Vening Meinesz' formulas by accounting for errors of truncation, potential coefficients and gravity data*. University of Uppsala, Institute of Geophysics, Department of Geodesy.
- Sjöberg, L. E.** (1995). The total terrain effect in the modified Stokes' formula. In Sünel, H. and Marson, I., editors, *Gravity and Geoid*, pages 616–623, Berlin, Heidelberg. Springer Berlin Heidelberg.
- Sjöberg, L. E.** (1999). The IAG approach to the atmospheric geoid correction in stokes' formula and a new strategy. *Journal of Geodesy*, 73(7):362–366.
- Sjöberg, L. E.** (2000). Topographic effects by the Stokes–Helmert method of geoid and quasigeoid determinations. *Journal of Geodesy*, 74(2):255–268.
- Sjöberg, L. E.** (2001). Topographic and atmospheric corrections of gravimetric geoid determination with special emphasis on the effects of harmonics of degrees zero and one. *Journal of Geodesy*, 75(5-6):283–290.
- Sjöberg, L. E.** (2003a). Ellipsoidal corrections to order e^2 of geopotential coefficients and Stokes' formula. *Journal of Geodesy*, 77(3-4):139–147.

- Sjöberg, L. E.** (2003b). A general model for modifying Stokes' formula and its least-squares solution. *Journal of Geodesy*, 77(7-8):459–464.
- Sjöberg, L. E.** (2003c). A solution to the downward continuation effect on the geoid determined by Stokes' formula. *Journal of Geodesy*, 77(1-2):94–100.
- Sjöberg, L. E.** (2004). A spherical harmonic representation of the ellipsoidal correction to the modified Stokes formula. *Journal of Geodesy*, 78(3):180–186.
- Sjöberg, L. E.** (2018). Topographic effects in geoid determinations. *Geosciences*, 8(4):143.
- Stokes, G. G.** (1849). On the variation of gravity on the surface of the Earth. *Trans. Camb. Phil. Soc.*, 8:672–695.
- Vajda, P. and Vaníček, P.** (1998). On the numerical evaluation of the truncated geoid. *Contributions to Geophysics and Geodesy*, 28(1):15–27.
- Valty, P., Duquenne, H., and Panet, I.** (2012). Auvergne dataset: testing several geoid computation methods. In *Geodesy for Planet Earth*, pages 465–472. Springer.
- Vanicek, P. and Krakiwsky, E. J.** (2015). *Geodesy: the concepts*. Elsevier.
- Vanicek, P., Zhang, C., and Sjöberg, L.** (1992). A comparison of Stokes's and Hotine's approaches to geoid computation. *Manuscr Geod*, 17(1):29–35.
- Yildiz, H., Forsberg, R., Ågren, J., Tscherning, C., and Sjöberg, L.** (2012). Comparison of remove-compute-restore and least squares modification of Stokes' formula techniques to quasigeoid determination over the Auvergne test area. *Journal of Geodetic Science*, 2(1):53–64.
- Zelin, G. and Yecai, L.** (1991). The determination of oceanic geoid using modified Hotine integral. In Rapp, R. H. and Sansò, F., editors, *Determination of the Geoid*, pages 86–94, New York, NY. Springer New York.

CURRICULUM VITAE



Name surname: Fatima Feyza Sakil

Date of birth and place: January 25, 1994, Denizli, Turkey

E-mail: ffsakil@gmail.com

Educational Status:

- **Master of Science (Exchange student)** September 2017 – January 2018: Tallinn University of Technology / Estonia, Department of Geodesy
- **Master of Science:** September 2016 - July 2018 (expected), Istanbul Technical University, Geomatics Engineering Programme.
- **Undergraduate:** September 2012- July 2016, Istanbul Technical University, Faculty of Civil Engineering, Department of Geomatics Engineering

Work Experience:

- September 2017 - Present : Istanbul Technical University - Gravity Research Group (ITU-GRG) , Istanbul-TURKEY, Researcher.
- July 2017 - January 2018: Local Guddy Inc., Istanbul-TURKEY, Community Manager
- June 2015 - September 2015: Institute of Geosciences of the Martin-Luther-University Halle - GERMANY, Intern
- January 2015 - February 2015: ESRI Turkey Technical Support Service, Ankara-TURKEY, Intern

Volunteer Works:

- Sports and Society Erasmus+ Project Berlin/Germany (August 2017)
- Assistantship in Kinder- und Jugendhaus e.V. in Halle/Saale/Germany (About children behavior and social activities) – (August 2015)
- Corporate Communication Executive in IAESTE Istanbul Technical University (2014 – 2015)
- Hand in Hand with Physics, Erasmus+ Project, Nyíregyháza / Hungary (2011)